MOIRÉ INTERFEROMETRY FOR OUT-OF-PLANE DISPLACEMENT MEASUREMENTS

by

Michael L. Basehore

Dissertation submitted to the Faculty of the

Virginia Polytechnic Institute and State University

in partial fulfillment of the requirements for the degree of

DOCTOR OF PHILOSOPHY

in

Engineering Mechanics

APPROVED:

D. Post, Chairman

C. W. Smith

E. G. Henneke, II

J. L. Lytton

M. W. Hyer

November, 1981

Blacksburg, Virginia

ACKNOWLEDGEMENTS

The author wishes to express his sincere appreciation to his committee chairman, Professor D. Post, for his support and guidance during the course of the author's academic and research endeavors at Virginia Polytechnic Institute and State University. Professor Post has unselfishly shared with the author his greatest attribute, creativity, an invaluable tool that few possess. In addition, the author wishes to express:

- his thanks to and the National Science Foundation for providing the funding for this work.
- his sincere thanks to Professor C. W. Smith for his overall support and numerous enlightening discussions in the area of Photomechanics.
- his appreciation to his committee members for their participation.
- his thanks to for his assistance.
- his appreciation to for typing the manuscript.
- his love and appreciation to his wife, , whose encouragement and understanding provided the strength required for this effort.

PREFACE

This dissertation is divided into three separate, yet interrelated sections dealing with the use of moiré interferometry to determine surface displacements. In Part I, it is shown analytically that wavefront warpage induced by specimen deformation provides sufficient information to determine both in-plane and out-of-plane displacement fields. This is followed by experimental corroboration.

Using Part I as a foundation, Part II details the development of an experimental technique which allows simultaneous determination of the in-plane and out-of-plane displacement fields. The method requires only one photographic exposure of the deformed specimen, with displacement information being extracted through the use of optical filtering.

In Part III, a procedure is described which has been developed for the production of high-frequency specimen gratings with a highly reflective surface.

Each of these three parts has been written to stand alone as a technical paper. For this reason, some repetition does occur in the dissertation.

TABLE OF CONTENTS

TABLE OF CONTENTS
(Continued)

LIST OF TABLES

LIST OF FIGURES

LIST OF FIGURES
(Continued)

LIST OF FIGURES
(Continued)

PART I

MOIRÉ METHOD FOR IN-PLANE AND OUT-OF-PLANE DISPLACEMENT MEASUREMENTS

SYNOPSIS--A high-frequency phase grating on a specimen surface is illuminated by oblique beams. Recordings of two diffracted beams by holographic interferometry reveal the wavefront changes N_a and N_b. In-plane displacements are proportional to $N_a - N_b$, while out-of-plane displacements are proportional to $N_a + N_b$. Experimental corroboration is presented.

INTRODUCTION

Moiré interferometry is a branch of photomechanics that utilizes a diffraction grating on the specimen; the grating is interrogated by two coherent beams that produce a pattern of two-beam interference fringes.[1] It is a relatively new technique. To date, it has been used to determine in-plane displacements of the specimen surface, but it is clear that the interfering beams also contain the out-of-plane displacement information.

This work is intended

(1) to show that in-plane displacements, U and V, and out-of-plane displacements, W, can be extracted independently from the wavefronts;

(2) to develop the relationships between wavefront parameters and these displacements; and

(3) to corroborate the relationships experimentally.

The experiments conducted here utilized holographic interferometry to record wavefront contours, and this approach may be used in practice. However, the author views the investigation as a foundation for a more efficient U, V, W

moiré technique currently under development. Equations (1.4) and (1.5) require subtraction and addition of parametric data and, in this sense, it is a moiré process. This, and plans to perform the addition by optical moiré methods, appears to justify the title.

Moiré interferometry is analogous in many ways to dual-beam speckle interferometry.[2] Sensitivity and precision are the same. Yet, a fully developed moiré capability is thought to offer certain advantages, since it is not restricted by limitations of range, contrast, and fringe localization associated with speckle.[3] The related holographic-interferometry method of Beranek can yield both in-plane and out-of-plane displacement fields.[4] This paper will show that moiré interferometry has the same potential.

MOIRÉ INTERFEROMETRY

In Fig. 1.1, the specimen has a diffraction grating of pitch 2g mm and frequency f/2 lines/mm formed on its surface. A collimated beam of light with a plane wavefront WF_0 is incident at angle α. If

$$\sin \alpha = \frac{f}{2}\lambda \qquad (1.1)$$

light of the -1 diffraction order emerges normal to the grating with wavefront $WF_{0,-1}$. If the grating is perfectly regular, $WF_{0,-1}$ is plane, but when it is deformed nonhomogeneously as a result of forces applied to the specimen, the wavefront becomes warped.

Simultaneously, let a coherent collimated beam with wavefront WF_1 strike the grating at symmetrical angle $-\alpha$. For this beam, light of the +1 diffraction order emerges with wavefront $WF_{1,1}$.

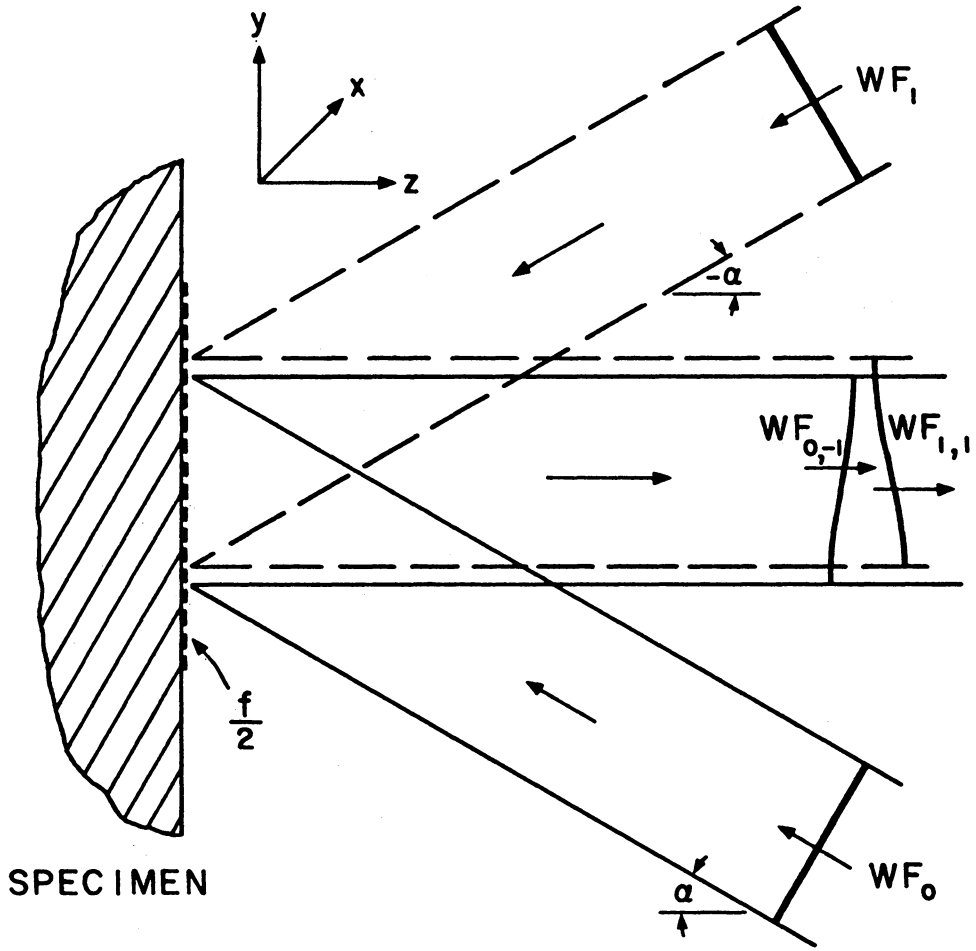

FIGURE 1.1. BEAMS DIFFRACTED FROM A DEFORMED SPECIMEN GRATING

This arrangement is recognized as a case of moiré interferometry with fringe-multiplication factor of 2. The two coherent incident beams generate a virtual grating of frequency f in their zone of intersection. This virtual grating, beating together with the deformed specimen grating of nominal frequency f/2, generates the moiré pattern of in-plane displacements U or V, depicting the x or y displacement field, respectively. The fringe order vs. displacement relationships are the same as for coarse moiré, viz.,

$$U = \frac{1}{f}(N)_x \qquad (1.2)$$

where N is moiré fringe order induced by the displacement.

Optically, fringe patterns are formed by interference between beams of the +1 and -1 diffraction orders. The moiré interferometry pattern is the contour map of the space between warped wavefronts $WF_{0,-1}$ and $WF_{1,1}$. Examples of moiré interferometry are shown in Fig. 1.8.

ANALYSIS

However, the shape of each of these wavefronts is influenced not only by the in-plane displacements of the specimen grating, but by its out-of-plane displacements, too. The wavefronts carry more information than that revealed by their subtractive moiré pattern. It is proposed now, that both the in-plane and out-of-plane displacement fields can be extracted from these wavefronts.

How can we produce a map of each wavefront? One way is double-exposure holographic interferometry. Using light with wavefront $WF_{0,-1}$ as the active beam, holographic exposures are made before and after the specimen is deformed. Upon reconstruction, the image of the specimen is covered by an

interference pattern representing the difference of optical-path lengths between plane wavefront $WF_{0,-1}$ occurring before deformation and warped wavefront $WF_{0,-1}$ after deformation. The result is a contour map of the warpage. Of course, holographic interferometry can be used in a second operation to produce a contour map of warped wavefront $WF_{1,1}$.

In practice, a perfect specimen grating is not required. If it is imperfect, the wavefront generated before deformation is not exactly plane, but this contribution to warpage is the same for the wavefronts occurring after deformation and its influence is cancelled. The holographic-interference patterns reveal only the contributions to wavefront warpage caused by the deformation. Interference patterns depicting this load-induced wavefront warpage are shown in Figs. 1.6 and 1.7.

But how can they be interpreted in terms of in-plane and out-of-plane displacements? By the grace of nature, the relationships are remarkably simple.

For the arrangement of Fig. 1.1, all in-plane displacements cause symmetrically opposite changes of the two wavefronts. The case of in-plane stretching in a vertical direction is illustrated in Fig. 1.2(a). Since the frequency of the grating becomes smaller, the angle of diffraction decreases for each of the two incident beams; emergent beams of +1 and -1 diffraction orders deviate symmetrically from the center line and wavefronts $WF_{0,-1}$ and $WF_{1,1}$ become symmetrically inclined.

On the other hand, out-of-plane rotation, δ, is illustrated in Fig. 1.2(b). Now, the beams diffracted in the +1 and -1 orders deviate to the same side of the center line. When δ is small, such that $\sin \delta = \delta$ and $\cos \delta = 1$ remain good

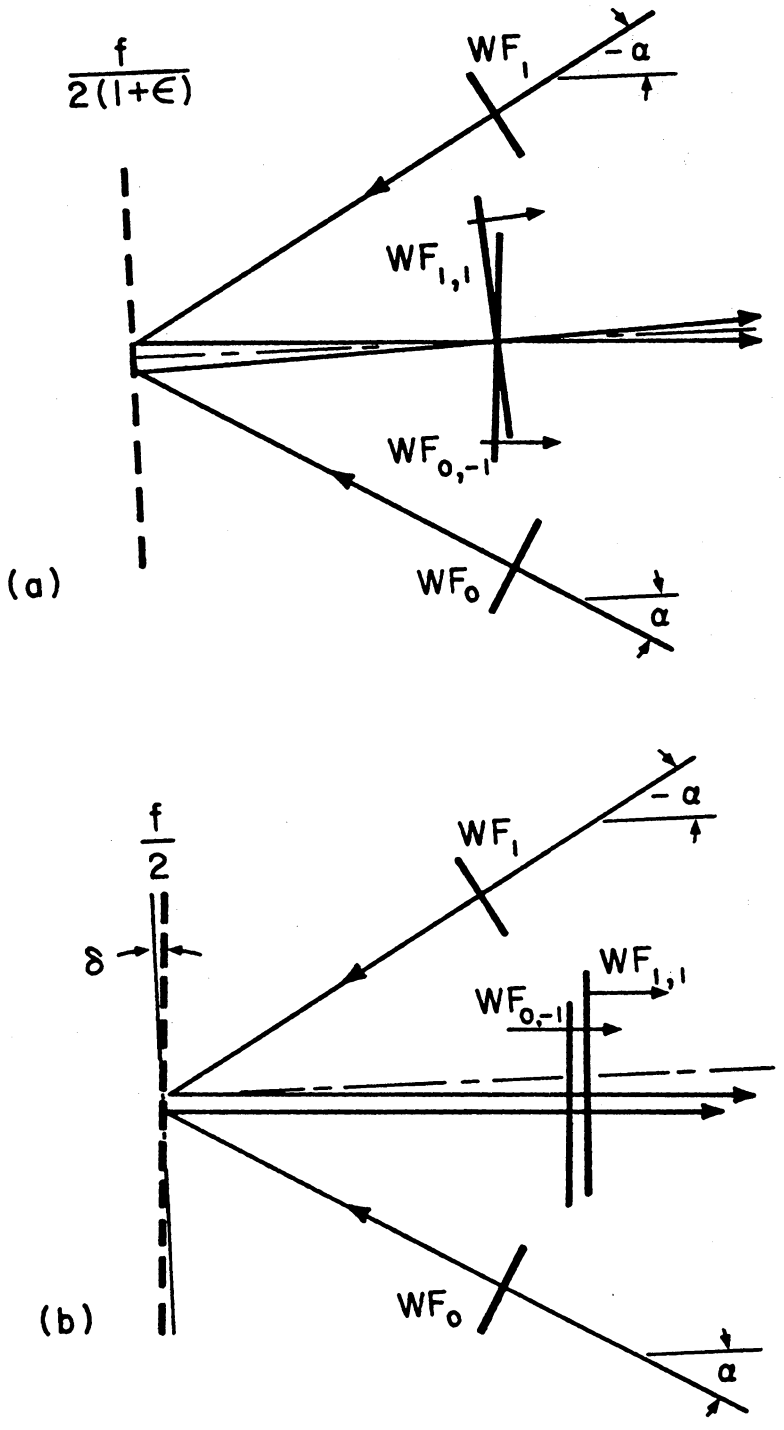

FIGURE 1.2. DIRECTIONS OF DIFFRACTED BEAMS AND THEIR WAVEFRONTS FOR (a) IN-PLANE STRETCHING WITH UNIFORM STRAIN ε, AND (b) OUT-OF-PLANE ROTATION δ OF THE SPECIMEN GRATING

approximations, wavefronts $WF_{0,-1}$ and $WF_{1,1}$ experience equal changes. They are shown separated in the figure, but actually they are coplanar.

In fact, this distinction applies to all movements of the grating. Figure 1.3 represents wavefront orientations for all components of motion of the grating. In each case, A represents the two superimposed wavefronts prior to displacement. The results of Fig. 1.2(a) for pure in-plane extensions are condensed in Fig. 1.3(a), showing symmetrical inclinations about A. In-plane rotation of the specimen grating, case (b), again causes symmetrical wavefront inclinations, but about an axis perpendicular to the grating lines. In-plane translation of the grating, case (c), causes symmetrical uniform separation of the wavefronts.

The results of Fig. 1.2(b) are condensed in (d), showing equal wavefront inclinations for rotation of the grating about an axis parallel to the grating lines. Again, the wavefronts are shown separated in Figs. 1.3(d), (e), (f) but, actually, they are coplanar. In (e), where out-of-plane grating rotation is about a perpendicular axis, the wavefronts again experience equal inclinations. Finally, for pure out-of-plane translation of the specimen grating, the two wavefronts experience equal uniform displacements from their original plane A.

The distinction between in-plane and out-of-plane motions is a remarkable property of the gratings. It can be utilized for quantitative measurements as follows.

Let λN_a represent the separation between $WF_{1,1}$ and its original plane A. Similarly, let λN_b represent separation between $WF_{0,-1}$ and A. For in-plane displacements [Figs. 1.3(a), (b), (c)], $N_a = -N_b$ for each point in the specimen's grating. For out-of-plane displacements [Figs. 1.3(d), (e), (f)], $N_a = N_b$. Superposition applies for small deformations and these relationships remain true for any

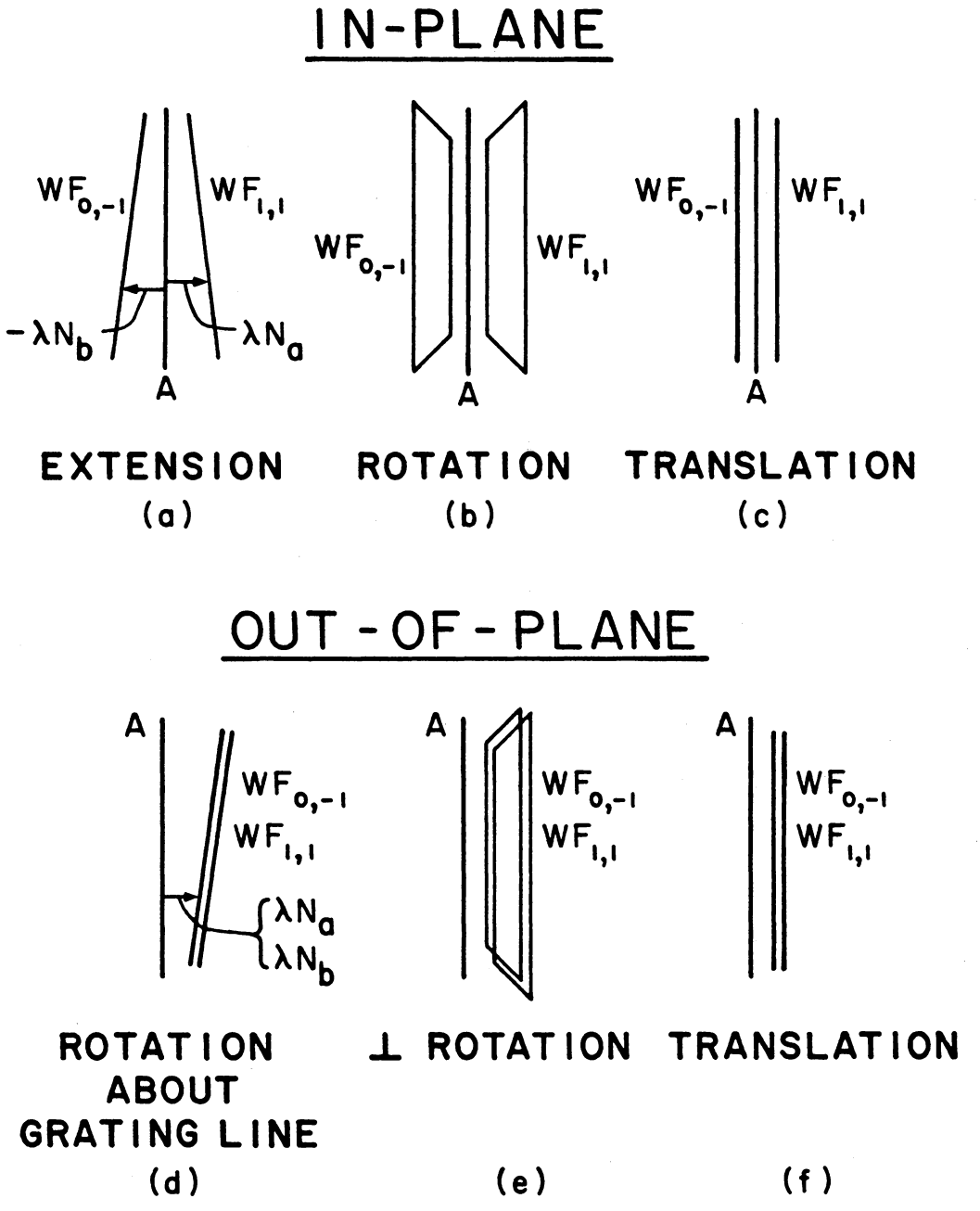

FIGURE 1.3. CHANGES IN WAVEFRONTS OF DIFFRACTED BEAMS CAUSED BY COMPONENTS OF MOTION OF SPECIMEN GRATING

combination of displacement components. Consequently, $N_a - N_b$ is a unique measure of in-plane displacements, while $N_a + N_b$ is a unique measure of out-of-plane displacements.

Since moiré fringe order N represents the separation between wavefronts $WF_{0,-1}$ and $WF_{1,1}$,

$$N = N_a - N_b . \tag{1.3}$$

By Eq. (1.2),

$$U = \frac{1}{f} N_x = \frac{1}{f}(N_a - N_b)_x$$

$$V = \frac{1}{f} N_y = \frac{1}{f}(N_a - N_b)_y \tag{1.4}$$

where f is given by Eq. (1.1); this is the frequency of the virtual grating that would be formed if incident beams carrying WF_0 and WF_1 are coherent and projected simultaneously, and subscripts x, y represent data taken with specimen grating lines initially perpendicular to the x and y directions, respectively.

The relationship for out-of-plane displacements may be derived from Fig. 1.4. A beam with wavefront WF_0 is incident upon the specimen grating and light from point B is diffracted to the observer. When B is displaced a distance W to B', the change of optical-path length (ΔOPL) between WF_0 and the observer is DB'B, or

$$\Delta OPL = W (1 + \cos \alpha).$$

For optical interferometry, one fringe represents a change of optical-path length of one wavelength, λ. In the case of out-of-plane displacements,

$$\Delta OPL = N_a \lambda = N_b \lambda ;$$

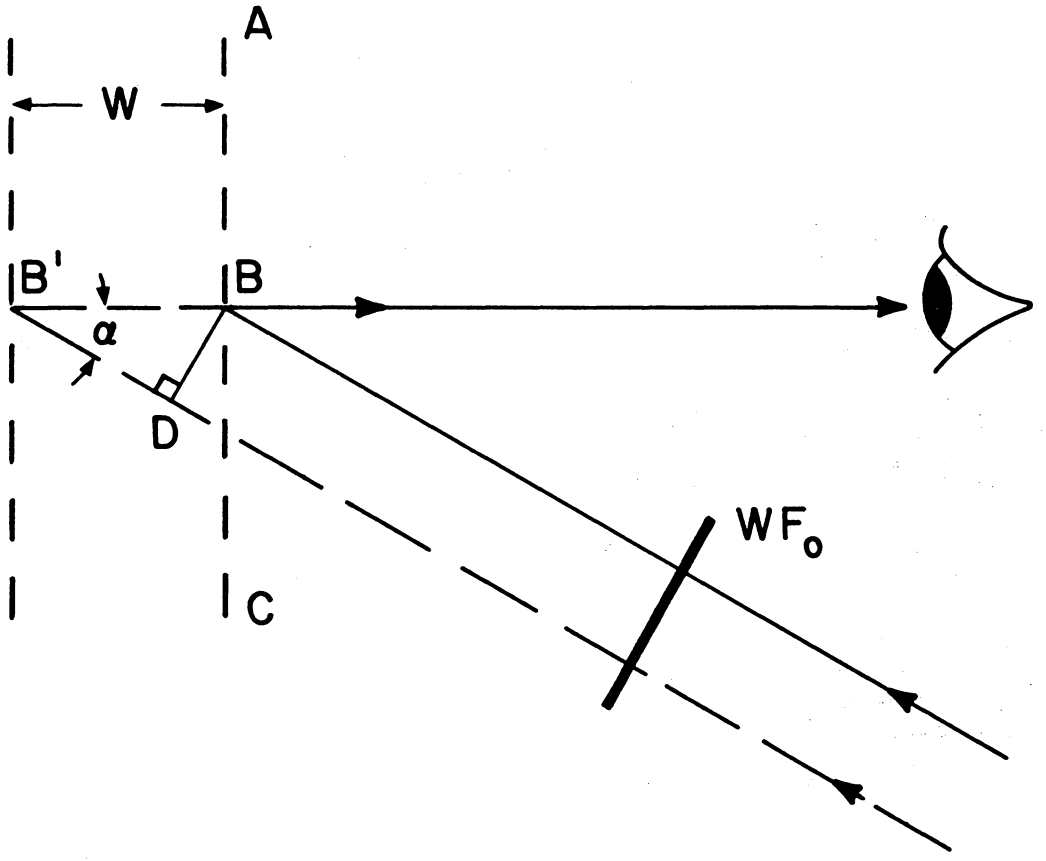

FIGURE 1.4. OPTICAL PATHS FOR DISPLACEMENT W

therefore

$$(N_a + N_b)\lambda = 2(\Delta OPL)$$

and

$$W = \frac{\lambda}{2(1 + \cos \alpha)} (N_a + N_b)_{x,y} . \qquad (1.5)$$

The subscripts x, y indicate that the data may be taken with specimen grating lines perpendicular to either the x or y directions, respectively.

Accordingly, two interferograms depicting N_a and N_b provide sufficient information to determine U and W, or V and W, throughout the field of view. The welcome conclusion is that their additive moiré gives out-of-plane displacements uniquely.

In the following experimental work, the separate problem of generating an optical contour pattern of $N_a + N_b$ is not undertaken. Instead, $N_a + N_b$ is determined numerically.

EXPERIMENTAL CORROBORATION

Plan

A strictly experimental approach was organized in which displacements measured by well-accepted prior experimental methods were used for comparison. The plan was to:

I. determine N_a and N_b by holographic interferometry;

II. determine N by moiré interferometry for identical loading conditions;

III. determine $N_\perp$ by normal-incidence holographic interferometry for identical loading conditions, where

$$W = \frac{\lambda}{2} N_{\perp} ; \tag{1.6}$$

from Eq. (1.5)

$$N_{\perp} = \frac{N_a + N_b}{1 + \cos \alpha} ; \tag{1.7}$$

IV. compare results of Step I to those of II and III by means of Eqs. (1.3) and (1.7).

An isotropic disk in diametral compression was chosen as test specimen. While the elasticity solution is known, precise duplication of theoretical loading conditions could not be assured. In addition, the test would be sensitive to inadvertent rigid-body tilting of the specimen during loading and inadvertent warpage of the midplane of the specimen. Consequently, comparison with experimentally determined actual displacement conditions was judged a superior approach.

Specimen and Specimen Grating

The disk used in the experiment was 50.8 mm (2 in.) in diameter and was machined from 9.5-mm (.375 in.) thick acrylic (PMMA) sheet stock. A phase grating was formed on the specimen surface by casting a thin film (approx. 0.03 mm) of silicone rubber between the specimen and a mold. The mold was a photographic plate containing a cross-line grating of f = 600 lines/mm (15,240 lines/in.). The method is described in Ref. 1.

Apparatus and Procedure

In order to assure equal specimen deformations for the three experiments listed above as I, II, and III, they were conducted simultaneously with the same

specimen and loading conditions. This necessitated an experimental setup and procedure which integrated the requirements of three separate experiments. Figure 1.5 is a schematic representation of the optical system used in this work.

For Method I, beams A and B illuminated the specimen grating. As illustrated in Fig. 1.1, light emerging from the grating in the -1 diffraction order from beam A and +1 diffraction order from beam B was intercepted by the hologram plate. Simultaneously, beams A' and B' were directed to the plate as reference beams. Four holograms were generated on the same plate; no-load and full-load holograms using beams A and A' and no-load and full-load holograms using beams B and B'.

Upon reconstruction with reference beam A', an interference pattern of N_a was formed in the camera. Similar reconstruction with beam B' yielded the interference pattern of N_b. While Fig. 1.5 shows the mirrors used to direct the reference beams to the hologram as being adjacent, in actual practice they were located one above the other. This created an angular difference between the reference beams which prevented 'crosstalk' during reconstruction. The resulting fringe patterns are shown in Figs. 1.6 and 1.7 for V, W and U, W interrogations, respectively.

Inherent in the same apparatus is the arrangement for Method II, moiré interferometry. Beams A and B were utilized while all other beams were blocked. No holographic plate was used. The camera was focused on the surface of the specimen so that the phase difference between emergent wavefronts $WF_{0,-1}$ and $WF_{1,1}$ was regenerated in its film plane to produce the pattern of moiré interferometry.

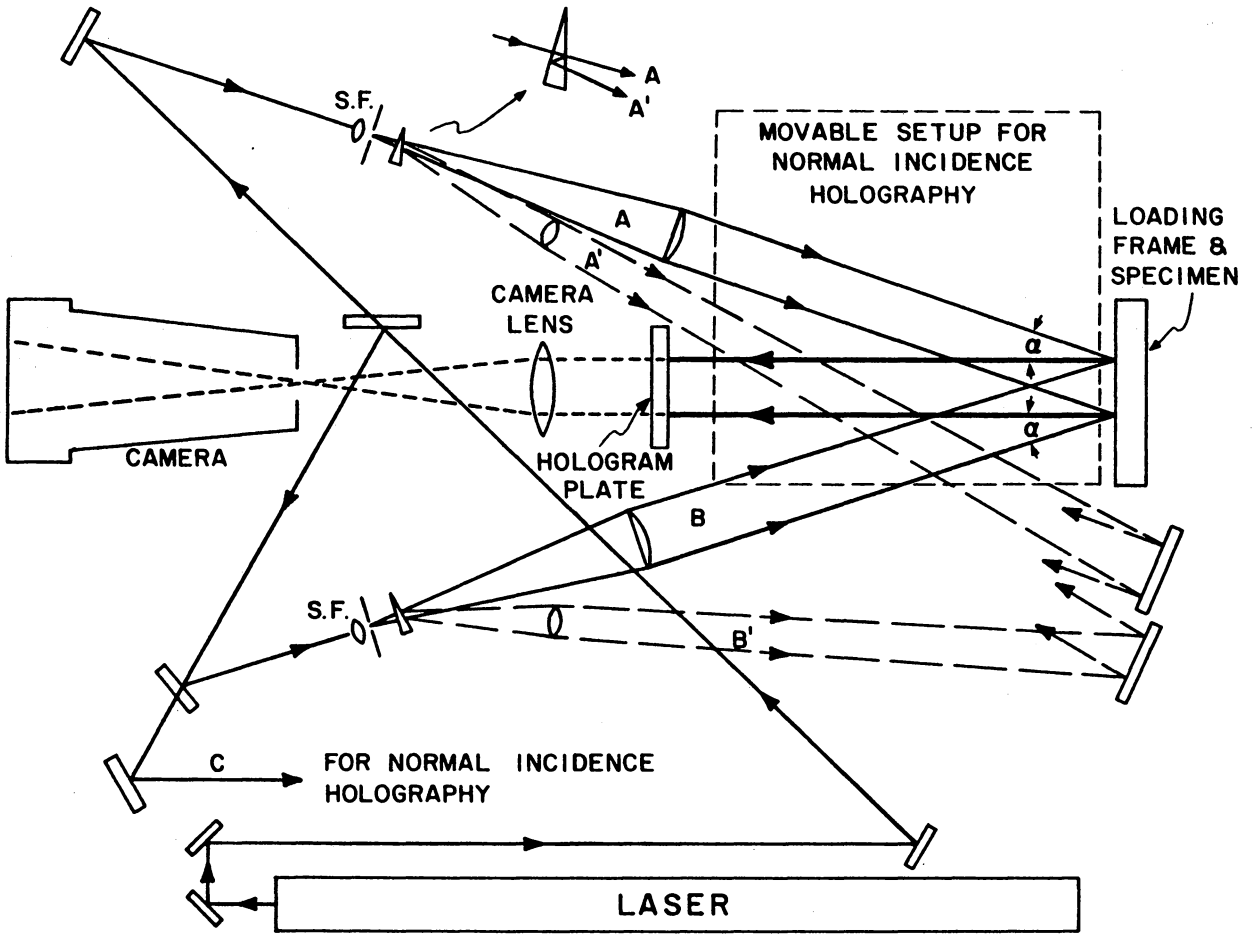

FIGURE 1.5. OPTICAL SYSTEM FOR EXPERIMENTAL OBSERVATIONS;
α = 18.0 DEG; S.F. INDICATES SPATIAL FILTER

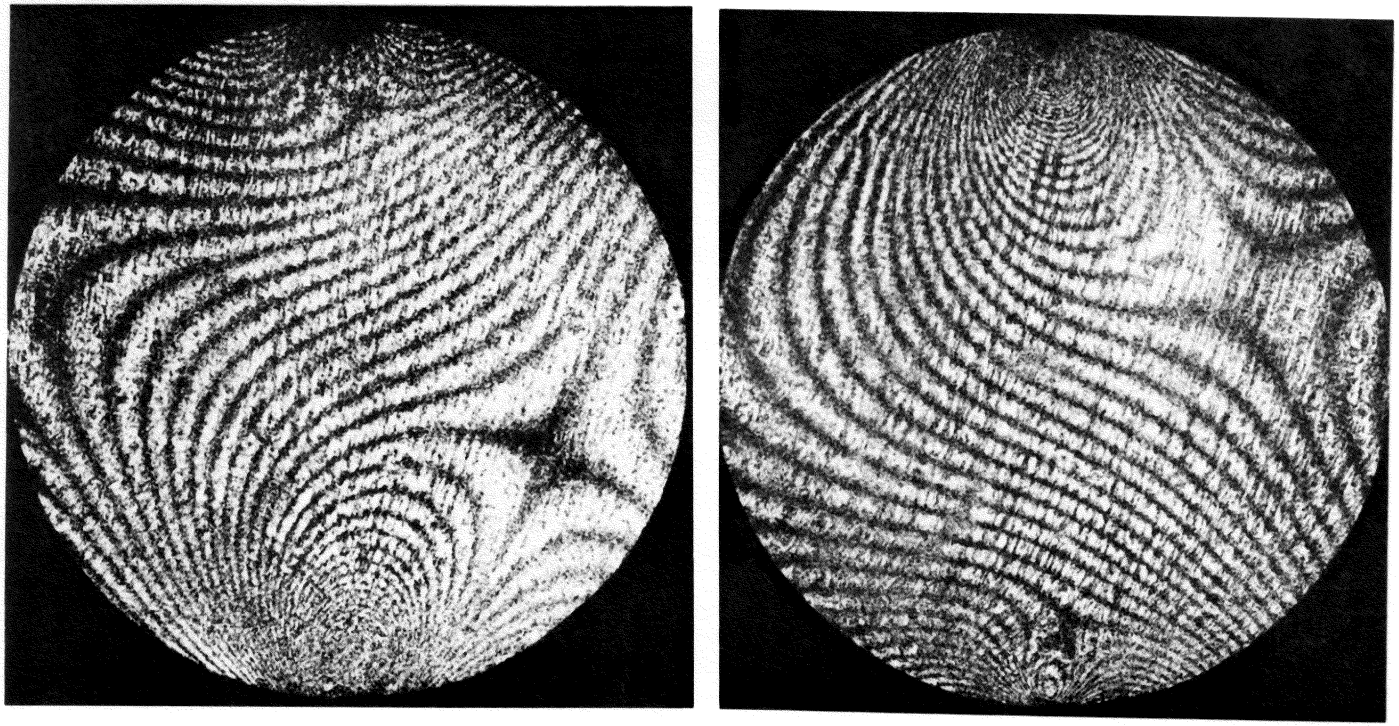

FIGURE 1.6. INTERFERENCE PATTERNS FOR V, W INTERROGATION.
LEFT: CONTOUR MAP OF $(N_b)_y$. RIGHT: $(N_a)_y$

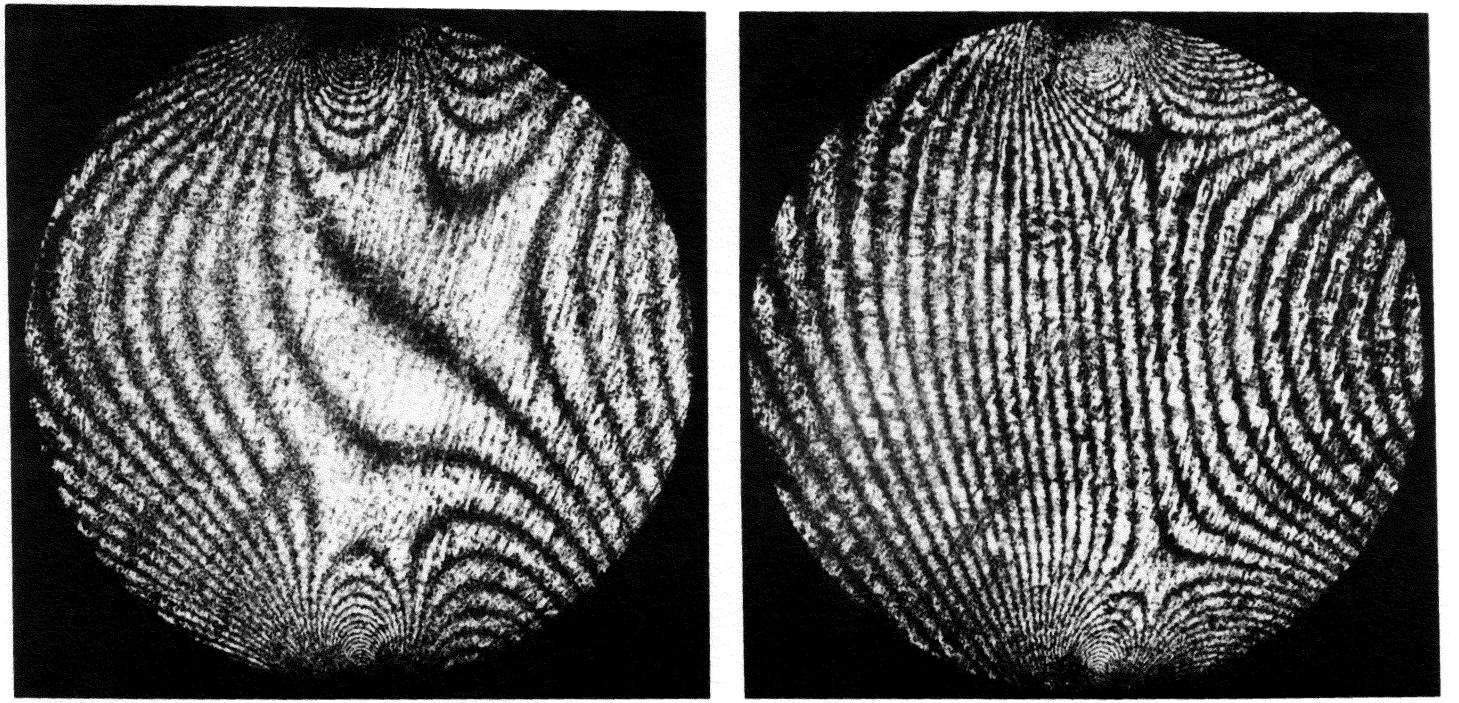

FIGURE 1.7. INTERFERENCE PATTERNS FOR U, W INTERROGATION.
LEFT: CONTOUR MAP OF $(N_b)_x$. RIGHT: $(N_a)_x$

A carrier pattern of pure rotation of approximately 8 fringes/mm was introduced by slightly raising the spatial filter through which beam A passes. Subsequent optical filtering removed the carrier pattern and enhanced fringe visibility for the patterns of in-plane displacements. A more detailed description of the optical filtering procedure can be found in Ref. 1. The fringe patterns are shown in Fig. 1.8 for x and y displacement fields.

Method III, normal-incidence holographic interferometry, was accomplished by means of an optical setup attached to a panel which could be moved into the area bordered by the dashed line in Fig. 1.5. The apparatus on the panel collimated beam C and directed it normal to the specimen surface. The reflected beam was incident upon a holographic plate attached to the panel. Also attached to the panel were optical elements which split beam C and directed a reference beam, C', onto the holographic plate. A hologram was made before and after the specimen was deformed by compressive loads. Upon reconstruction with beam C', the pattern revealed the out-of-plane displacement fringes, $N_{\perp}$, caused by deformation of the specimen.

The procedure for completing all of the multiple exposures for the three methods in the same specimen-loading cycle was as follows. The movable panel containing the normal-incidence holography setup was positioned outside of beam A. Beam C and reference beams A' and B' were blocked. A no-load exposure was made on photographic film in the camera for the moiré interferometry. A holographic plate was placed in the holder. Beams B and B' were blocked and a no-load holographic exposure was made using beams A and A'. This step was repeated using beams B and B'. The no-load hologram was covered and the panel containing the normal-incidence holography setup was slid into place. A no-load

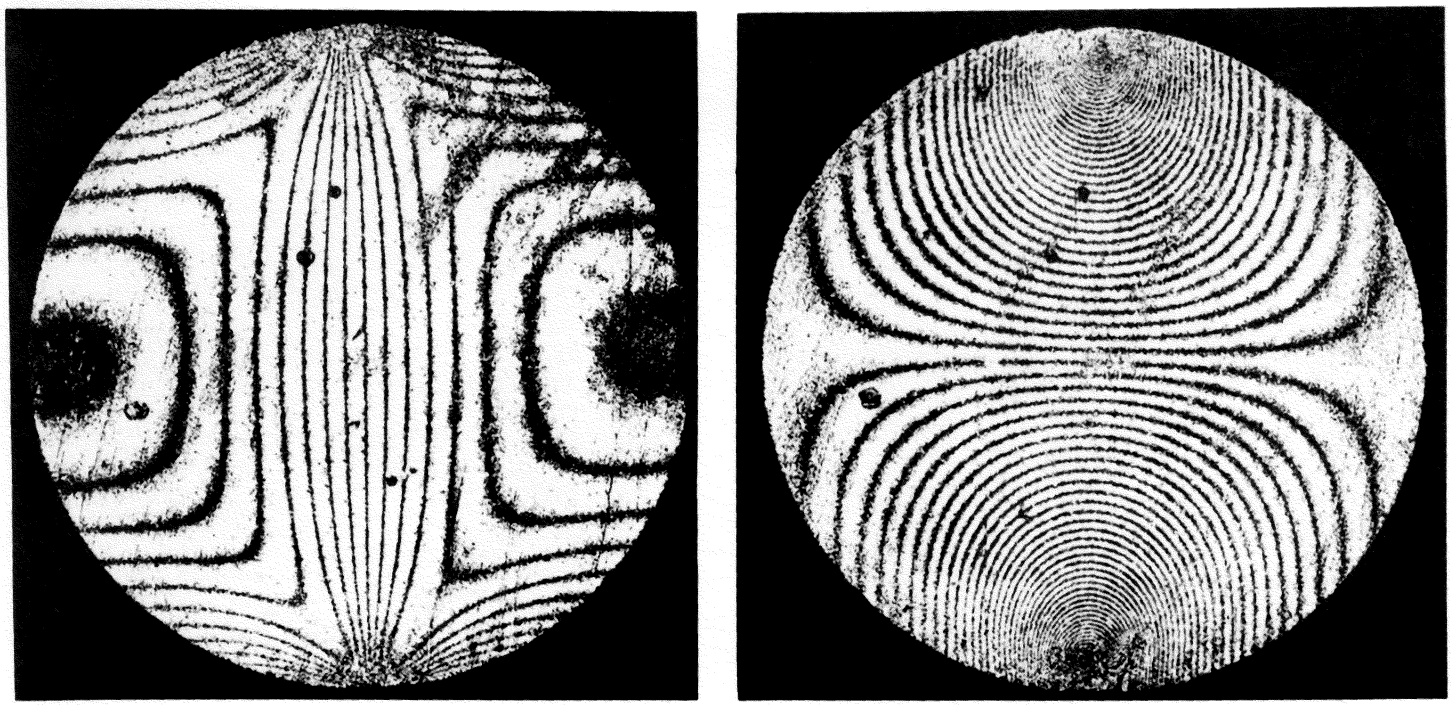

FIGURE 1.8. CONTOUR MAPS OF DISPLACEMENT FIELDS N_x (LEFT) AND N_y (RIGHT) BY MOIRÉ INTERFEROMETRY

exposure was made using beams C and C'. A predetermined load was applied to the specimen and a second exposure was made on the holographic plate. The normal-incidence setup was removed and the hologram plate shown in Fig. 1.5 was uncovered. Second exposures were made with beams B and B' and then with beams A and A'. The plate was removed from the holder and the second exposure was made on the photographic film in the camera for moiré interferometry.

The loading frame, complete with loaded specimen, was then rotated 90 deg to interrogate the orthogonal elements of the cross-line grating. The procedure described above was repeated except that all first exposures were full-load exposures, followed by a second no-load exposure.

Careful study of the results reveals that the load increments were not identical for both interrogations. It suggests that the original and final low-load levels, the so-called 'no-load' conditions for the two tests, were not equal. However, this load discrepancy had no influence on the experimental corroboration, since comparisons may be made for any load increment.

RESULTS

The results of Methods I, II, and III were educed from the fringe patterns and compared for two lines across the specimen, the horizontal diameter AB and the 45 deg diagonal CD. Graphs of fringe order vs. position were drawn for the two lines for each fringe pattern. For Method I, smooth curves were drawn through the data points, and fringe orders N_a and N_b taken from them were used to calculate the parameters of Eqs. (1.3) and (1.7).

The point of zero displacement may be chosen arbitrarily and the center of the disk was selected here. Results are shown in Figs. 1.9-1.12, where in-plane

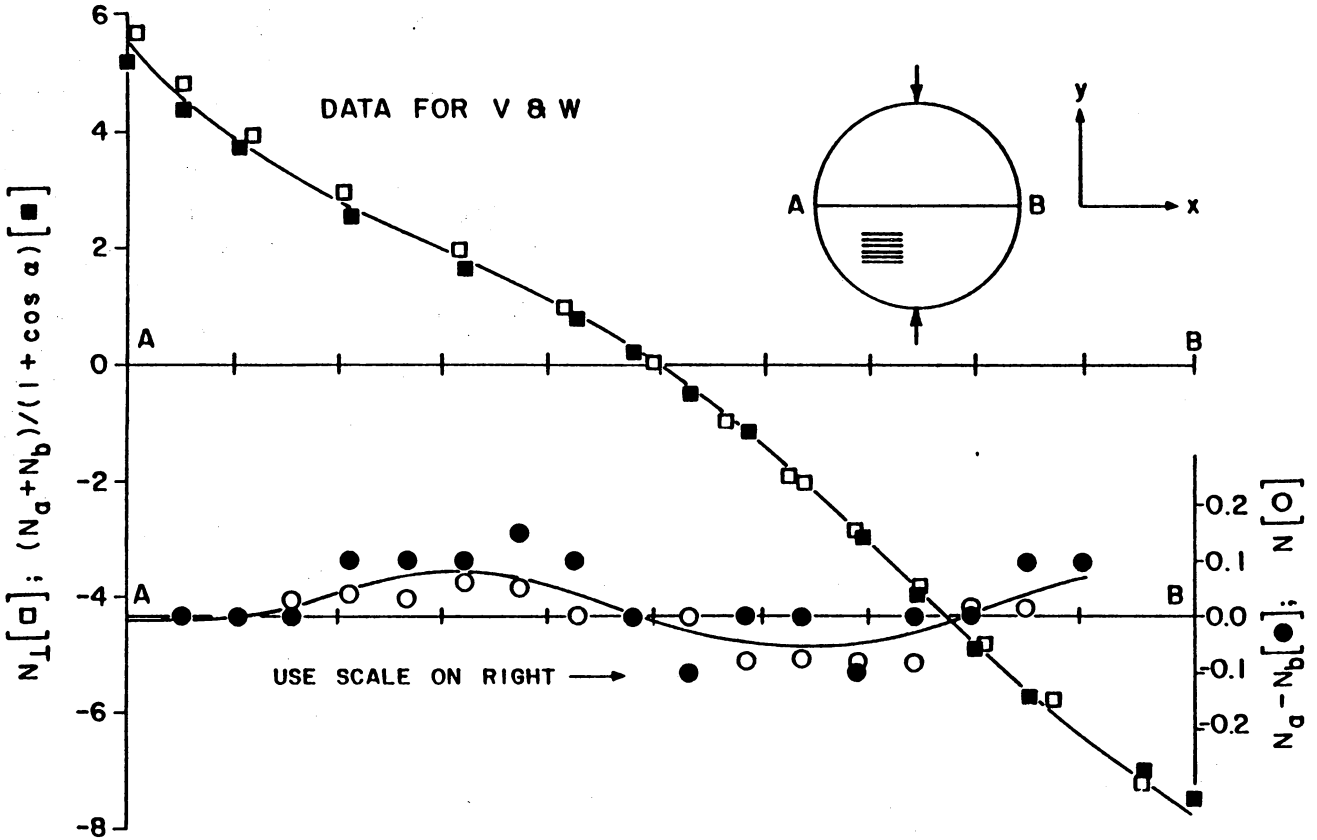

FIGURE 1.9. CORROBORATION OF EQS (1.3) AND (1.7) FOR LINE AB; V, W INTERROGATION

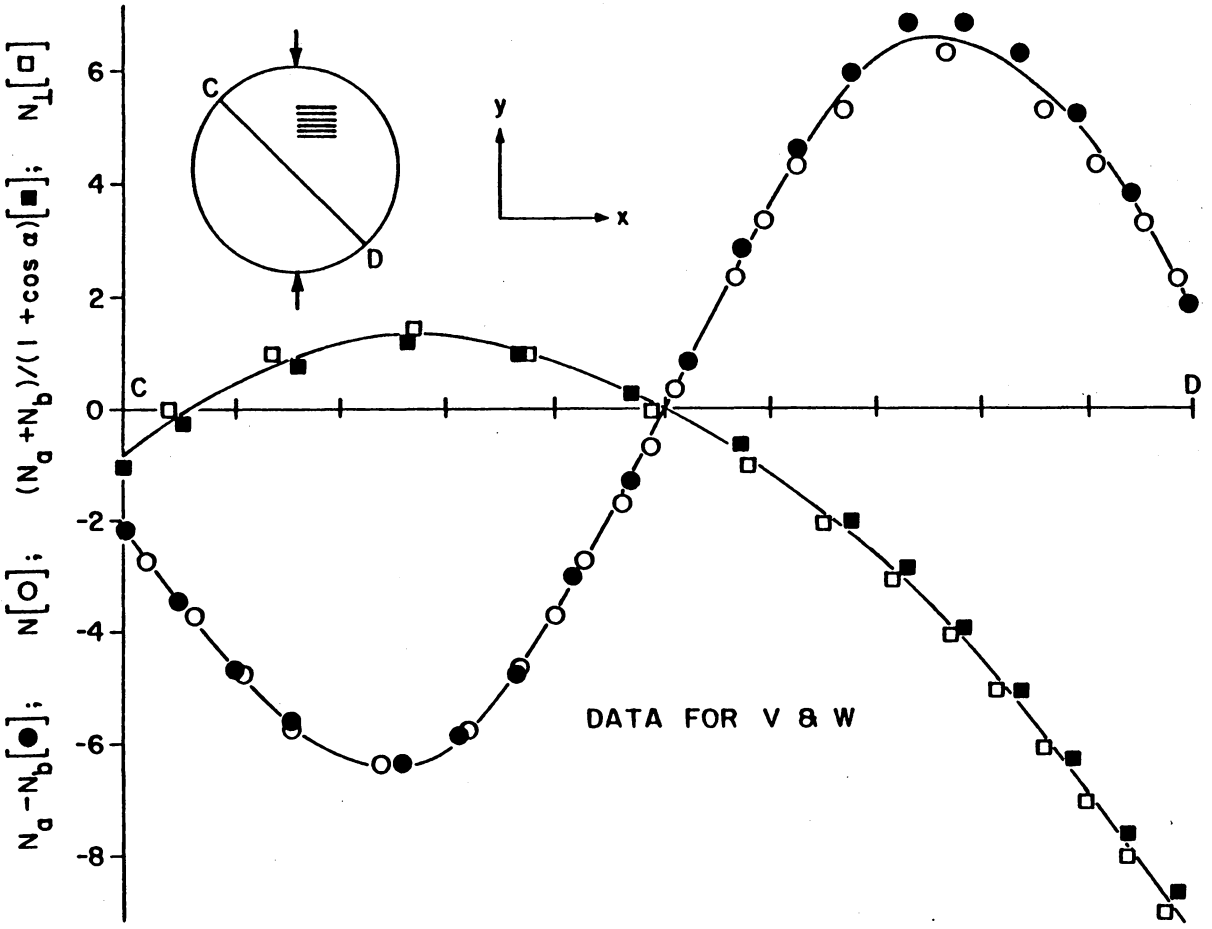

FIGURE 1.10. CORROBORATION FOR LINE CD; V, W INTERROGATION

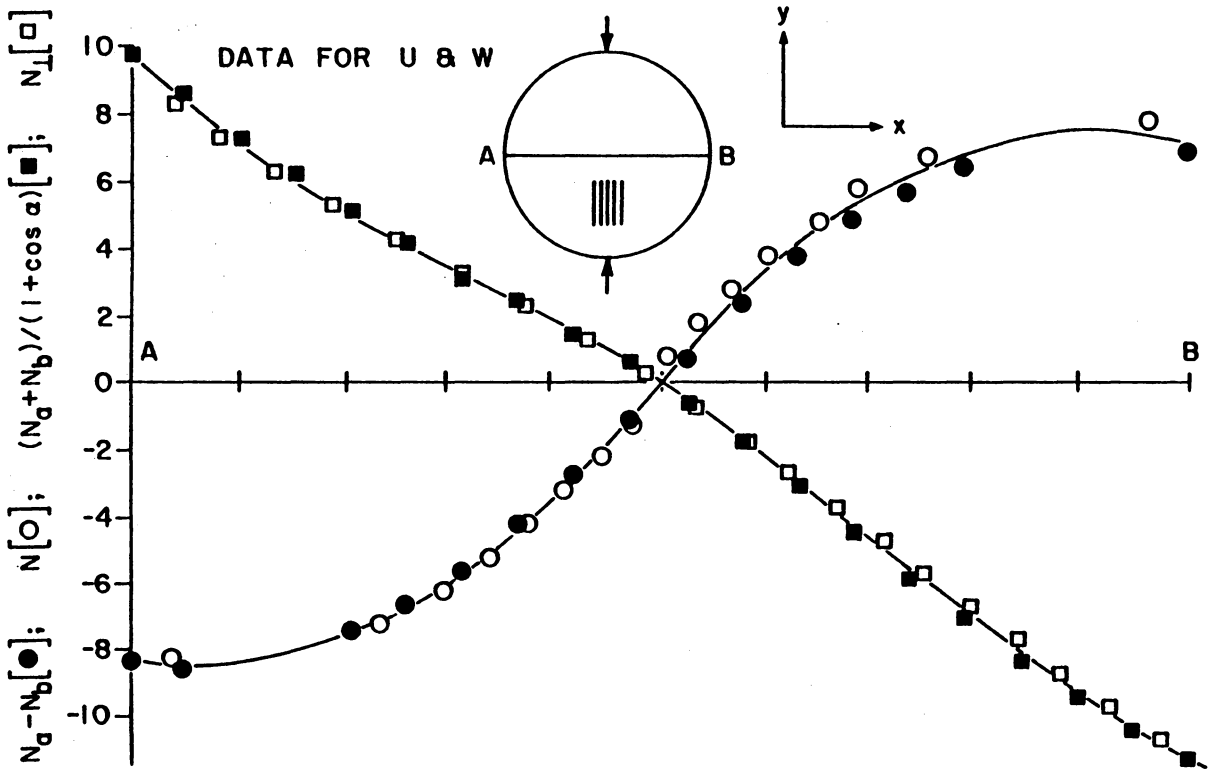

FIGURE 1.11. CORROBORATION FOR LINE AB; U, W INTERROGATION

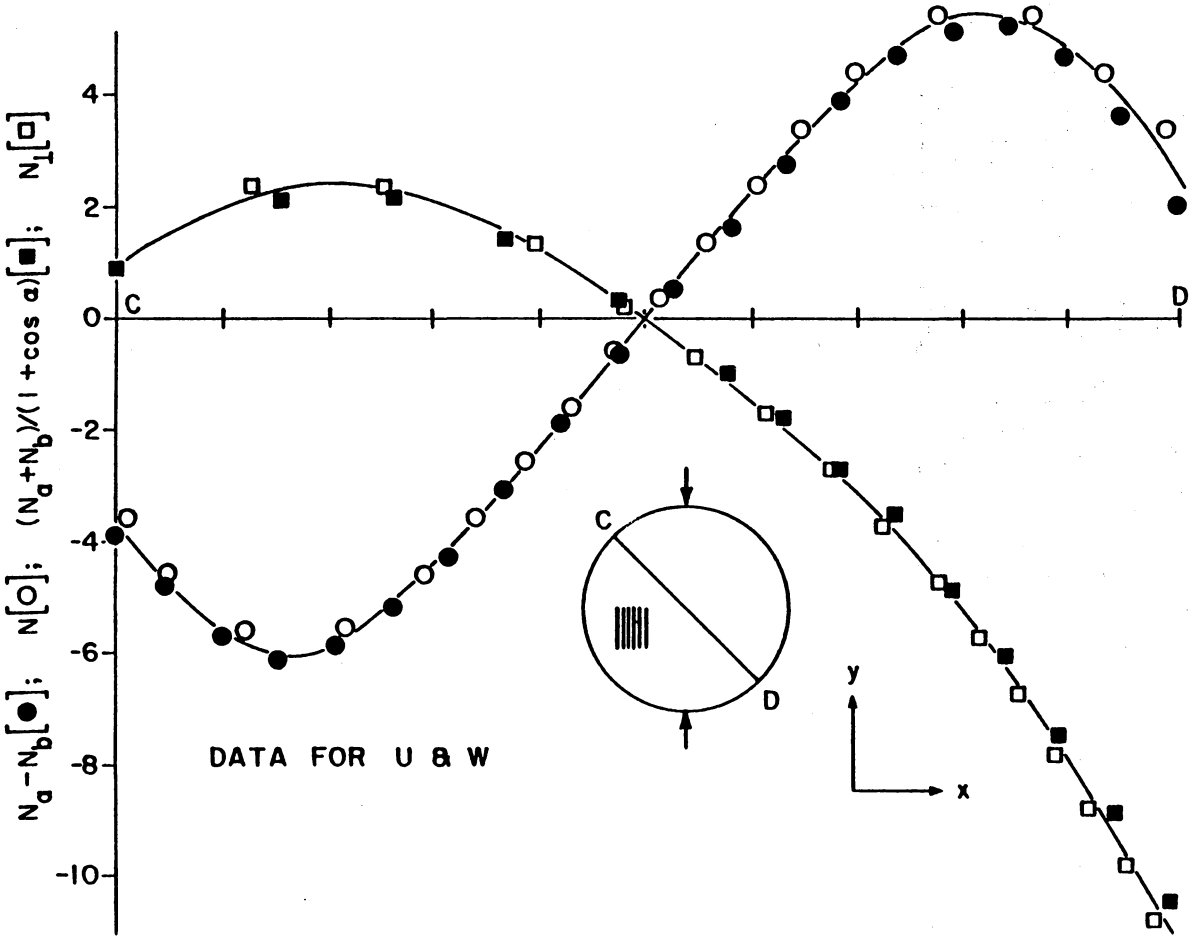

FIGURE 1.12. CORROBORATION FOR LINE CD; U, W INTERROGATION

parameters are illustrated by circles and out-of-plane parameters are represented by squares.

The similarity of results is striking. Note the enlarged scale in Fig. 1.9 for in-plane results. The difference between the two methods was less than one-tenth of a fringe order; in terms of displacement, this maximum difference is 8.3×10^{-5} mm (3.3×10^{-6} in.). All the graphs showed excellent corroboration.

Regarding experimental accuracy, the greatest problem was encountered in establishing the location of reference lines AB and CD on the fringe-pattern photographs. The inexact locations of these lines appear to be responsible for most of the deviation between Methods I, II, and III. The graphs show that deviations are mostly systematic, not random, and could be further reduced by small adjustments in locations of the lines on the fringe photographs. Of course, this source of experimental error could have been eliminated completely by the simple expedient of scribing lines AB and CD on the specimen prior to the experiment.

The fringe patterns and the graphs reveal that the specimen experienced some out-of-plane rigid-body tilting and some warpage of its midplane. This is noted from Fig. 1.12, for example. It shows that the out-of-plane displacements (proportional to $N_{\perp}$) are not equal at points C and D, thus indicating tilting of the disk. It shows, too, that out-of-plane displacements are not symmetrical, indicating midplane warpage of the disk.

CONCLUSIONS

Equations (1.3) and (1.7) are developed by rational analysis and are corroborated by excellent experimental agreement with proven methods.

It has been shown that the two interfering beams used for moiré interferometry contain information from which both in-plane and out-of-plane displacements can be extracted independently. Relationships between the wavefront parameters and the displacements reveal remarkably simple results. If the wavefront warpages of the two diffracted beams are characterized by fringe orders, N_a and N_b, the in-plane displacements are proportional to $N_a - N_b$, while out-of-plane displacements are proportional to $N_a + N_b$.

PART II

U,W DISPLACEMENT FIELDS OBTAINED SIMULTANEOUSLY BY MOIRÉ INTERFEROMETRY

SYNOPSIS--A high frequency phase grating on a specimen surface is illuminated by two oblique beams. Wavefront warpage of these beams induced by specimen deformation provides sufficient information to determine U and W displacement fields. A moiré-interferometric technique utilizing a third auxiliary beam yields contour maps of these two warped wavefronts in a single photographic record. Optical filtering performed in a separate procedure extracts whole-field fringe patterns of U and W.

INTRODUCTION

Moiré interferometry is rapidly becoming a viable means of determining surface displacements with a very high degree of sensitivity. Recent efforts have shown that moiré fringes of excellent quality can be obtained with sensitivity to in-plane displacements as high as 1/1670 mm per fringe (1/42,420 inch per fringe).[5] It is feasible that through the use of current techniques the theoretical sensitivity limit of $\lambda/2$ per fringe can be approached closely, where λ is the wavelength of the incident light.

To date the majority of studies utilizing the moiré method have dealt with the determination of in-plane displacements U and V of a specimen surface, although a few investigations have demonstrated the feasibility of using moiré techniques to determine out-of-plane displacements W as well. Sciammarella, Di Chirico, and Chang[6] used a double exposure technique with higher diffraction orders to obtain out-of-plane displacements with a sensitivity of 1/160 mm per fringe (1/4000 inch per fringe). The author, in Part I of this dissertation, prepared the foundation for the current work. Prescribing the normal arrange-

ment of moiré interferometry, Fig. 2.1, he showed that the two wavefronts emerging from a deformed specimen grating can be used to determine not only the in-plane displacements, but the out-of-plane displacements as well. In this previous work, holographic interferometry was used to capture the wavefront contours. Subsequent addition and subtraction of the resulting parametric data led to out-of-plane and in-plane displacements, respectively.

The present work is intended to provide a technique where both the addition and subtraction are performed automatically by optical moiré methods. The objective is to extract two distinct fringe patterns: (1) a contour map of in-plane displacements U or V (depicting the x or y displacement field, respectively), and (2) a contour map of out-of-plane displacements W (representing the z displacement field).

MOIRÉ INTERFEROMETRY

In moiré interferometry, a diffraction grating of frequency f/2 lines/mm formed on a specimen surface is illuminated by two coherent beams, A and B, at symmetrical angles α and $-\alpha$. This is depicted in Fig. 2.1. If

$$\sin \alpha = \frac{f}{2}\lambda \qquad (2.1)$$

the two coherent incident beams generate a virtual grating of frequency f in their zone of intersection. If the specimen grating is deformed by loads applied to the specimen, this virtual grating together with the deformed specimen grating produces the moiré pattern of in-plane displacement, U or V.

For present purposes, it is necessary to examine the effect of the specimen grating more closely. When Eq. 2.1 is satisfied, light of the +1 and -1

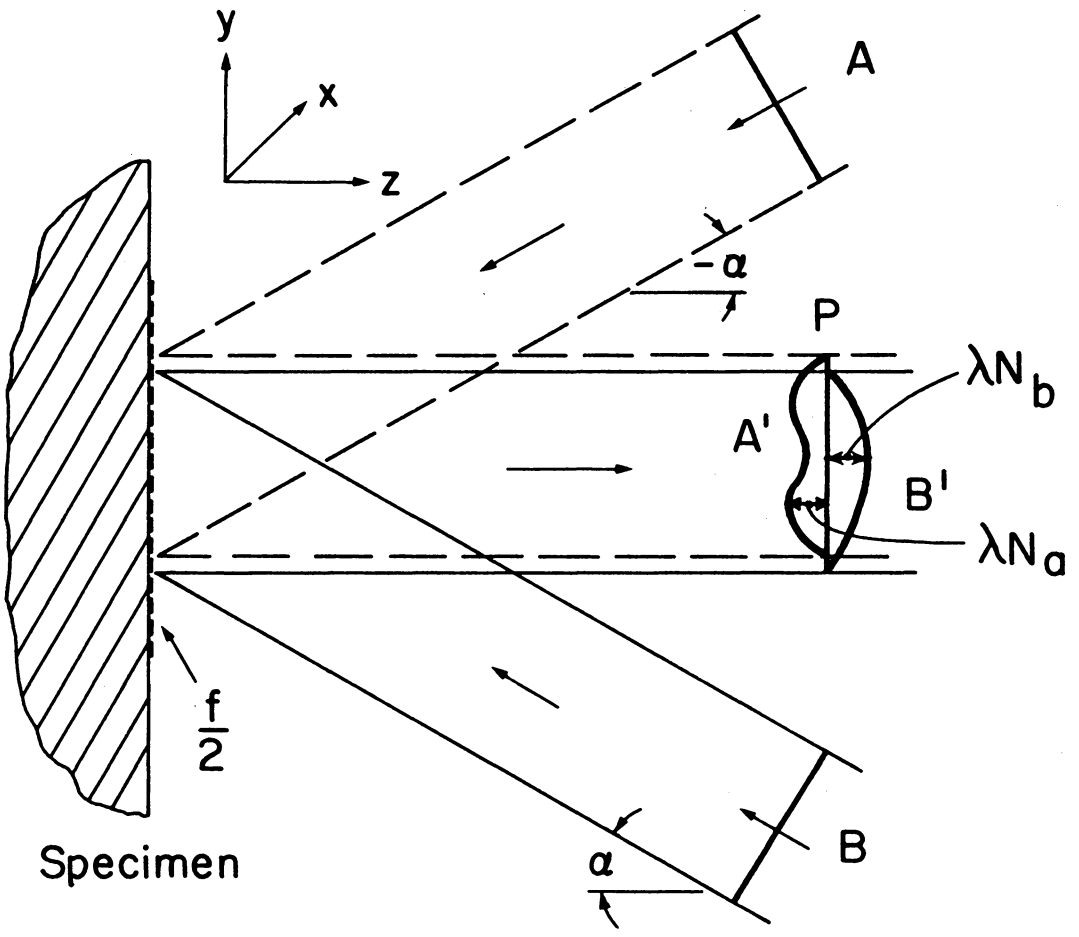

FIGURE 2.1. SYMMETRICAL ARRANGEMENT OF MOIRÉ INTERFEROMETRY

diffraction orders emerges normal to the grating. If the specimen grating is perfectly regular, both of these beams have plane wavefronts, as illustrated by line P in Fig. 2.1. However, if the grating is deformed by forces applied to the specimen, both of the emerging wavefronts become warped. Let λN_a represent the separation between warped wavefront A' and its original plane P. Similarly, let λN_b represent the separation between warped wavefront B' and plane P. Reference 7 shows that in-plane displacements of the specimen grating result in symmetrically opposite warpages of wavefronts A and B, i.e., $N_a = -N_b$. Conversely, out-of-plane displacements cause wavefronts A and B to experience equal warpages, or $N_a = N_b$. Thus, $N_a - N_b$ is a unique measure of in-plane displacements, while $N_a + N_b$ is a unique measure of out-of-plane displacements.

These parameters determine the U and W displacement of the specimen surface by Eq. (1.4) and (1.5) rewritten here as

$$U = \frac{1}{f}(N_a - N_b) \tag{2.2}$$

and

$$W = \frac{\lambda}{2(1 + \cos \alpha)} (N_a + N_b) \ . \tag{2.3}$$

Here f is the virtual grating frequency given by Eq. 2.1 and grating lines are initially perpendicular to the x-direction. Of course, if the grating lines are initially perpendicular to the y-direction, in-plane displacement V would be determined as well as redundant W data.

The subtractive parameter, $N_a - N_b$, can be recognized as being equal to the moiré fringe order N associated with the classical fringe order vs. displacement relationship

$$U = \frac{1}{f} N \quad . \tag{2.4}$$

The fringe order N can be obtained using current moiré interferometry techniques.[1,5] Convenient means to produce the fringe pattern corresponding to the additive parameter, $N_a + N_b$, must now be investigated. The following sections describe two experimental techniques that can be used.

EXPERIMENTAL APPARATUS

The experimental arrangement is illustrated in Fig. 2.2. It is the same apparatus as described in Ref. 5, except for the addition of the auxiliary mirror. The auxiliary mirror is uncoated, but it has a dielectric reflectance of about 4%. It is slightly wedge-shaped so the reflection from its rear surface emerges in a different direction and can be disregarded. When the frequency of the specimen grating is precisely one-half the frequency of the virtual reference grating, and the lines of the specimen grating are exactly parallel to the lines of the virtual grating, emerging beams a, b, and o (depicted as rays in Fig. 2.2) will be coincident. However, if the specimen is rotated slightly about an axis normal to its surface, active beams a and b deviate slightly in symmetrically opposite directions with respect to auxiliary beam o. When the three beams are intercepted by a lens as illustrated in Fig. 2.3, they are converged to three distinct points on the camera aperture plate.

Scheme I

The additive quality can be manifest in the following manner. Let the aperture plate of Fig. 2.3 be positioned to allow light from beams a and o to enter the camera for the first exposure [Fig. 2.4(a)]. Reposition the aperture to

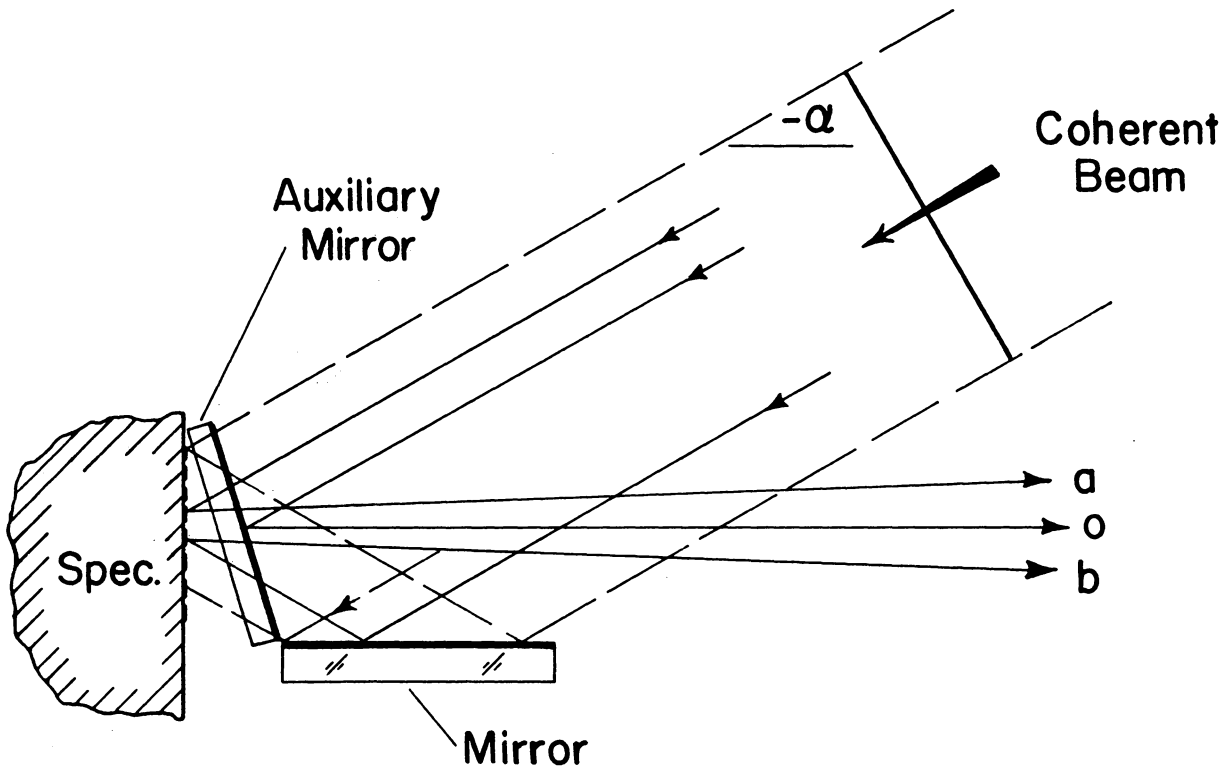

FIGURE 2.2. EXPERIMENTAL ARRANGEMENT. THE FULL MIRROR GENERATES A SYMMETRICAL INPUT BEAM AT ANGLE + α AND THE AUXILIARY PARTIAL MIRROR PROVIDES AUXILIARY BEAM o

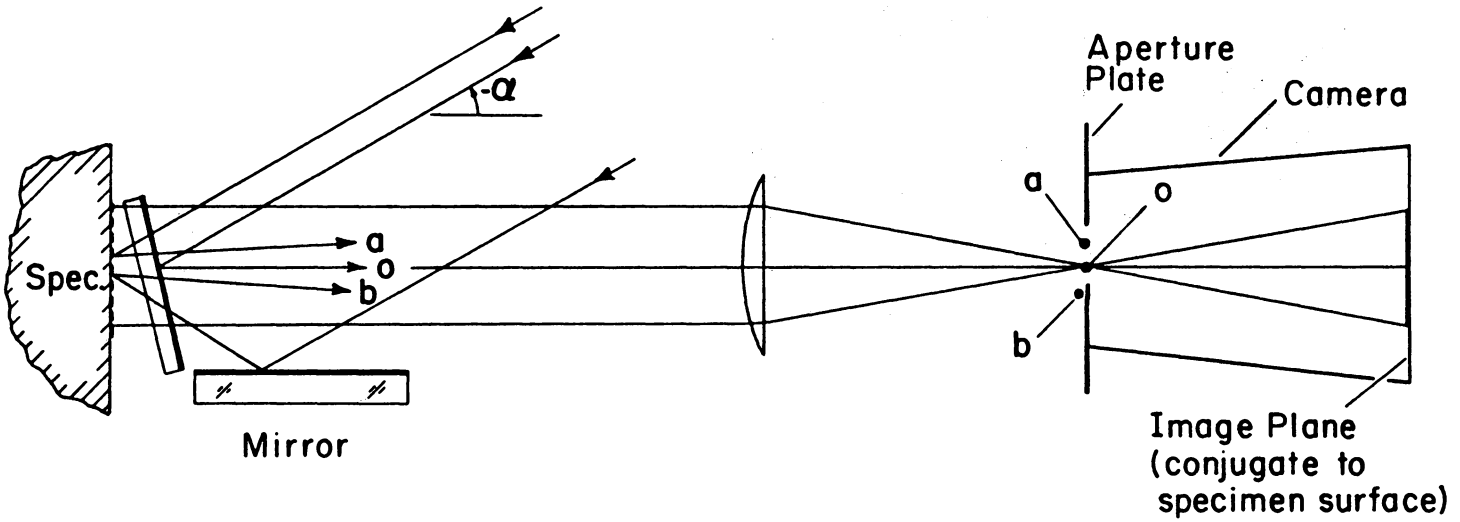

FIGURE 2.3. BEAMS REPRESENTED BY RAYS a, b, AND o CONVERGE TO DIFFERENT POINTS ON THE CAMERA APERTURE PLATE

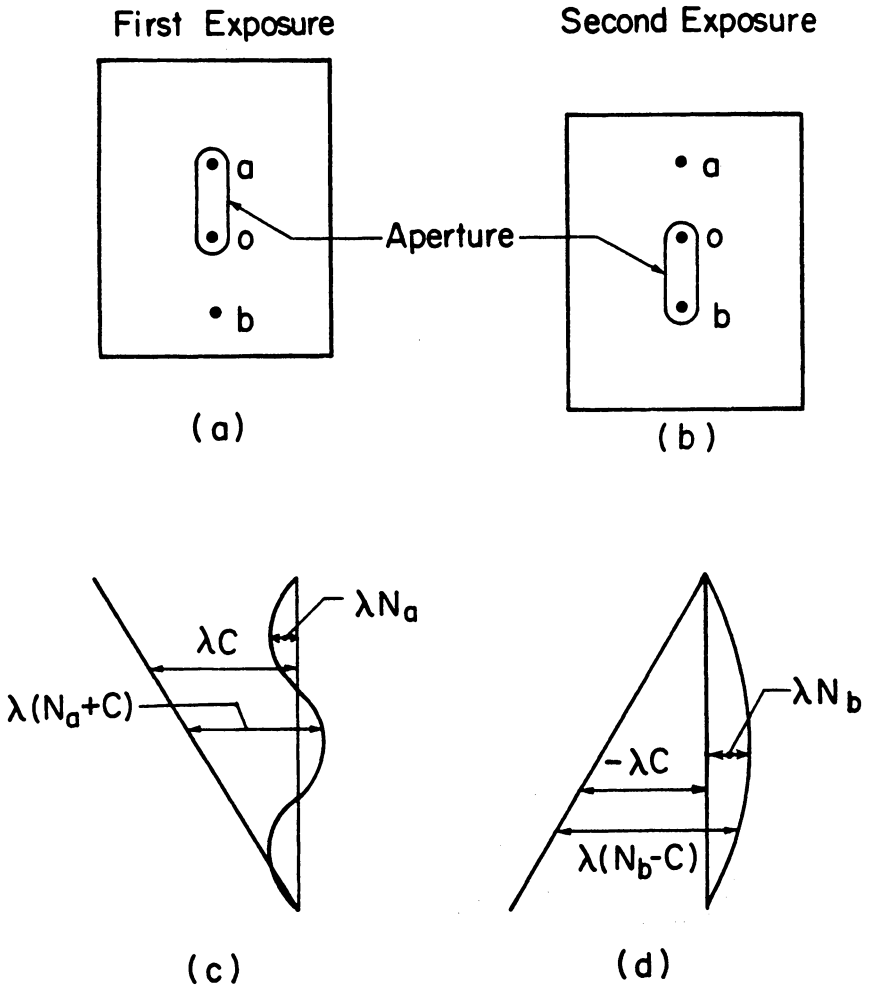

FIGURE 2.4. IN SCHEME I, TWO BEAMS AND THEIR CORRESPONDING WAVEFRONTS ARE ADMITTED INTO THE CAMERA FOR EACH EXPOSURE

allow light from beams b and o to enter the camera [Fig. 2.4(b)] for a second exposure on the same film. With the aid of Fig. 2.4(c), it can be seen that interference of beams a and o produces a contour map of $N_a + C$. Here, C represents the uniform contours of a carrier pattern caused by the angular deviation between beams a and o, and N_a represents the contours of warped wavefront a, where warpage is introduced by the deformation of the specimen grating. Similarly, interference between beams b and o produces a contour map of $N_b - C$ as shown in Fig. 2.4(d). This carrier pattern is designated as -C since the angular deviation of beams b and o is opposite that between beams a and o.

With the lens (Fig. 2.3) adjusted to focus an image of the specimen surface on the camera back, the two patterns are coincident. This superposition of interference patterns $N_a + C$ and $N_b - C$ on the same negative creates a moiré pattern. It is well known that both additive and subtractive fringes exist simultaneously in a moiré pattern, although only one of them has good visibility.[8] The additive moiré consists of a family whose fringe orders, N', are defined as the sum of the fringe orders of the superimposed patterns, which in the present case is

$$N' = (N_a + C) + (N_b - C)$$

or

$$N' = N_a + N_b \ . \tag{2.5}$$

The subtractive moiré consists of lines whose fringe orders, N, are defined as the difference of the fringe orders of the superimposed patterns

$$N = (N_a + C) - (N_b - C)$$

or

$$N = N_a - N_b + 2C \quad . \tag{2.6}$$

Since the angular deviations between beams a and o and between b and o yield carrier patterns, C, of high frequency (e.g. 20 fringes/mm), N consists of very closely spaced fringes in which the moiré phenomenon is not visible. In this case, the additive moiré yields coarser, visible fringes of $N_a + N_b$. This is the desired pattern, from which out-of-plane displacements are determined by Eq. 2.3.

The in-plane displacement field can also be obtained. Beam o is blocked and light from beams a and b is allowed to enter the camera aperture. A no-load exposure is made resulting in an interference pattern of $N_a - N_b + 2C$. The specimen is loaded and a second exposure is made on the same film. After developing, this film is placed in an optical filtering system such as described in Ref. 1. This optical filtering process removes the carrier pattern, 2C, and enhances the contrast of the desired interference pattern, $N_a - N_b$. The resulting fringe pattern is a measure of the change of in-plane displacement between the no-load and load cases.

Scheme II

Although the technique described above is capable of yielding both the in-plane and out-of-plane displacement fields, two qualities can be enhanced. In Scheme I,

(I) The double exposure required in the load condition precludes transient dynamic investigations.

(2) If the W displacement field for the no-load condition exhibits fringes, their fringe orders must be subtracted manually to determine the load-induced W field.

Scheme II provides an alternative experimental scheme that circumvents these drawbacks.

The same experimental setup as described for Scheme I is utilized. However, the auxiliary mirror is rotated about an axis parallel to the lines of the gratings, causing beam o to deviate horizontally from beams a and b. The positions of the beams converged to the camera aperture plate are illustrated in Fig. 2.5(a). It should be noted that the distances identified as y_1, y_2, and x in Fig. 2.5(a) are not exacting quantities that require precision adjustments. Indeed, it is not even necessary that $y_1 = y_2$ for this scheme, although for later operations it is convenient if $y_1 \approx y_2 \approx x$. The only requirement is that they remain constant for both the no-load and load exposures described in the following sections.

Light from all three beams is allowed to enter the camera, resulting in three superimposed interference patterns, depicted in Fig. 2.5(b). When the specimen is loaded and wavefronts A' and B' become warped, these patterns represent:

(1) Interference between beams a and o, producing a contour map of $N_a + C_x + C_{y_1}$. Once again, N_a represents the contours of warped wavefront a, or A', while C_x and C_{y_1} are components of a carrier pattern caused by orthogonal angular deviations between beams a and o.

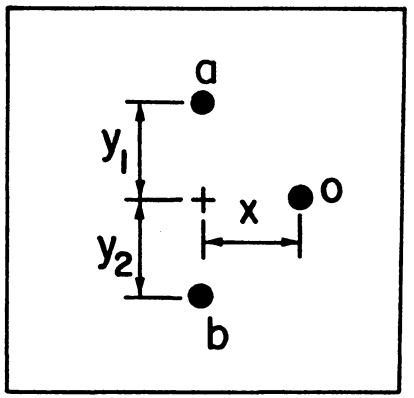

Aperture Plate
of Fig. 2.3

(a)

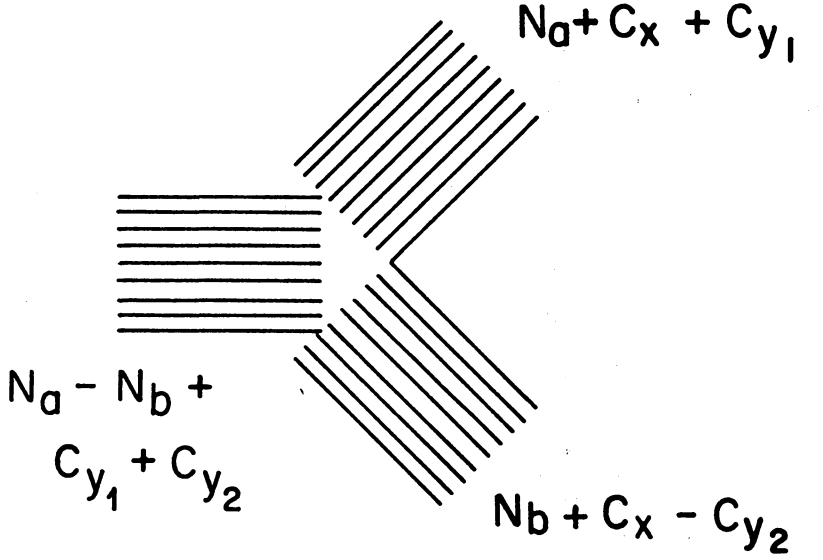

Interference Patterns
in Film Plane
of Fig. 2.3

(b)

FIGURE 2.5. IN SCHEME II, ALL THREE BEAMS ARE ALLOWED TO PASS SIMULTANEOUSLY THROUGH THE APERTURE PLATE OF FIG. 2.3, TO PRODUCE THREE SUPERIMPOSED FRINGE PATTERNS ILLUSTRATED IN (b)

(2) Interference between beams b and o, producing a contour map of $N_b + C_x - C_{y_2}$.

(3) Interference between beams a and b, resulting in a contour map of $N_a + C_{y_1} - (N_b - C_{y_2})$ or $N_a - N_b + (C_{y_1} + C_{y_2})$.

Although shown separately in Figure 2.5(b), the three interference patterns are in fact superimposed over the entire image. It will be shown that this single photographic record, combined with a corresponding no-load pattern, provides $N_a - N_b$ and $N_a + N_b$. Optical filtering is used to extract the information.

Optical Filtering

An optical filtering technique, such as described in Ref. 1, can be used to isolate the warped wavefronts in such a manner that they may be judiciously recombined to yield the subtractive and additive parameters. A photographic film is exposed in the moiré interferometry system and developed. The resulting photographic negative contains the three interference patterns described above. In each, the carrier pattern is dominant, with wavefront warpage information manifest as irregularities in the otherwise uniform carriers. When placed in the optical filtering system illustrated in Fig. 2.6, each of the three patterns behaves as a coarse diffraction grating. Beams emerge from the negative in the various directions of the diffraction orders of the three carrier gratings and are converged to separate points on the aperture plate of Fig. 2.6. Figure 2.7 portrays the array of bright spots of light seen on the plate. Although shown here as distinct points of light, they are in fact local clusters of points. The information that each of the beams carries, i.e., the warped wavefronts, causes each beam to converge to a small cloud of points in the aperture plane.

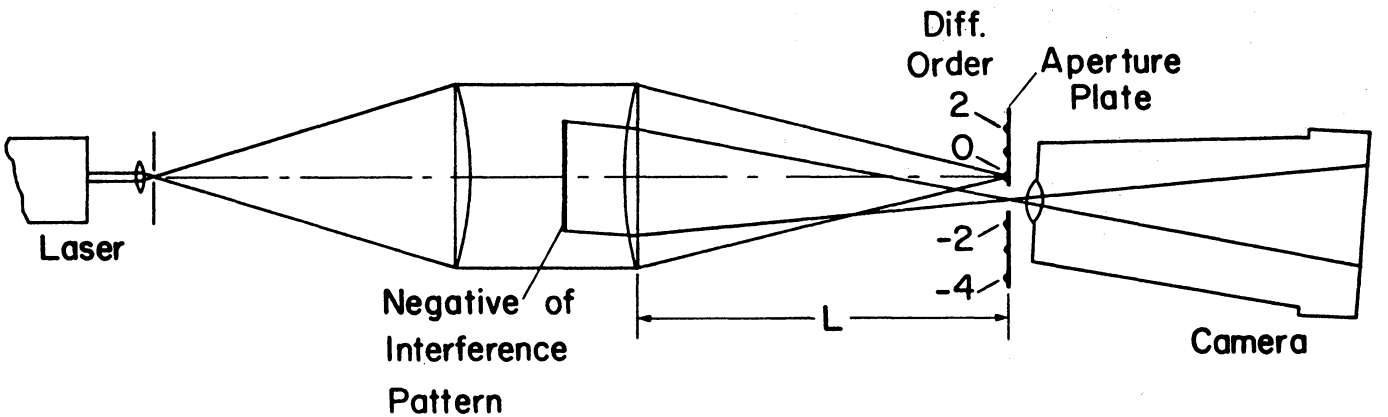

FIGURE 2.6. ARRANGEMENT FOR OPTICAL FILTERING OF THE MANY BEAMS DIFFRACTED BY THE NEGATIVE. ONE OR TWO SELECTED BEAMS ARE ALLOWED TO PASS THROUGH THE APERTURE PLATE

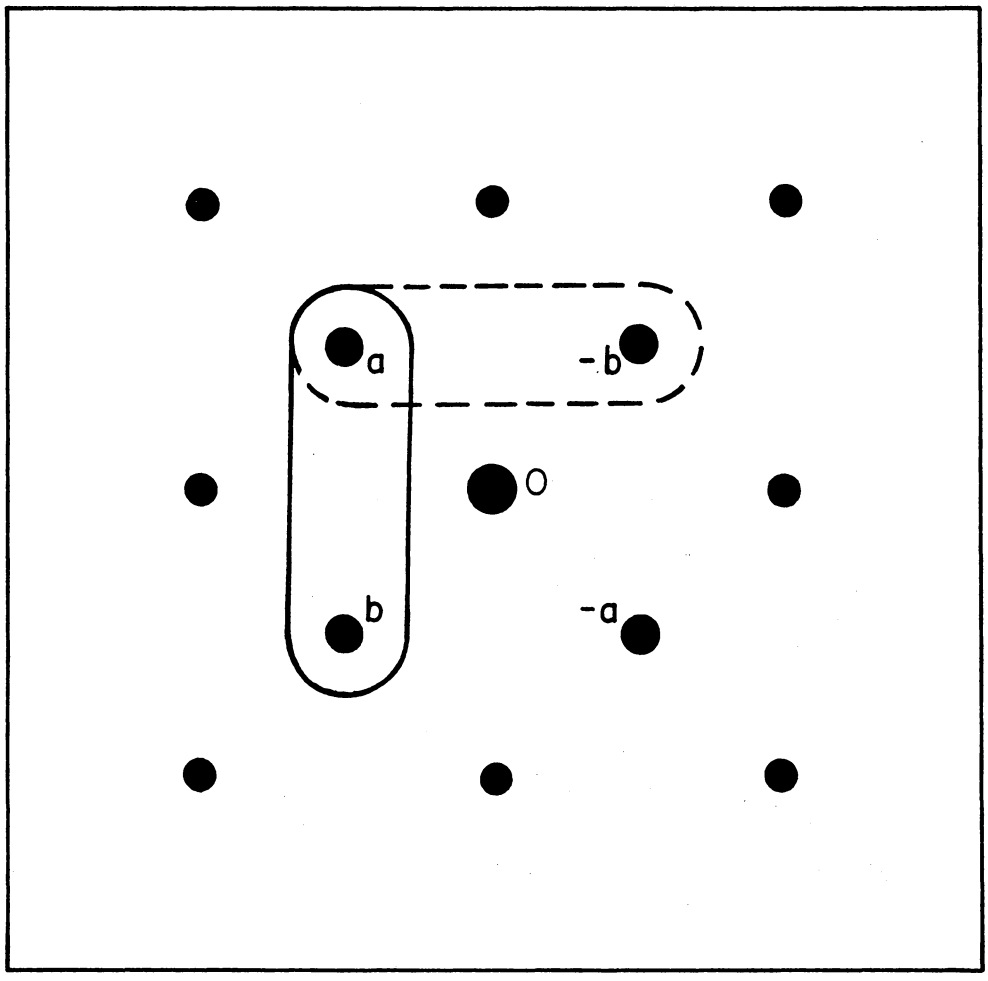

Camera Aperture Plate
of Fig. 2.6

FIGURE 2.7. IN THE FIRST OPTICAL FILTERING STEP OF SCHEME II, NUMEROUS DIFFRACTED BEAMS FALL ON THE APERTURE PLATE OF FIG. 2.6. BEAMS a AND b, AND SUBSEQUENTLY a AND -b, ARE ADMITTED INTO THE CAMERA AND PHOTOGRAPHED ON SEPARATE FILMS

The points are labeled in Fig. 2.7 according to the information contained in the converged beam. Light crossing through 0 is from the zeroth diffraction order of each grating and carries no information. Cloud "a" denotes that light passing through this zone is the reconstruction of the warpage of wavefront A'. The cloud symmetrically opposite is labeled "-a" because it is the -1 diffraction order and therefore possesses a wavefront which is inverted (or the mirror image) with respect to wavefront a.[9] Similarly, b and -b are comprised of light that reconstructs the wavefront warpage of beam B'. For purposes of clarity, light of other diffraction orders, including higher order and combined order diffractions, is not labeled.

An aperture illustrated by the solid line in Fig 2.7 is used first, allowing light from beams a and b to enter the camera. The image formed on the film plane is a contour map of the separation between the two wavefronts; in this case $N_a - N_b + C_1$, where C_1 represents a carrier pattern caused by the angular deviations between beams a and b. This pattern is photographed. Next, an aperture is used which allows light from beams a and -b to enter the camera. This aperture is represented by the dashed line in Fig. 2.7. The interference between these two beams produces a contour map of $N_a - (-N_b) + C_2$. The pattern is photographed on a separate film. It should be noted that carrier patterns in the raw data and the filtered patterns are interrelated. For example, if unit magnification is used in all photographic steps, and if

$$y_1 = y_2,$$

then $$C_1 = 2C_{y_1}$$

and $$C_2 = 2C_{y_2}.$$

These two patterns allow extraction of the load-induced U and W displacement fields. The steps described above for the load condition are also followed for the initial or no-load condition. Thus, four negatives are produced. The load and no-load negatives of $N_a - (-N_b) + C_2$ are superimposed and inserted together in the same optical filtering system (Fig. 2.6) where the first diffraction order of the carrier is observed. The result is a moiré pattern in which the carrier contribution is cancelled and the influence of the no-load fringe pattern is eliminated. This is the load-induced pattern of $N_a + N_b$. By Eq. 2.3, this yields the W displacement field. Similarly, the load and no-load patterns of $N_a - N_b + C_1$ are superimposed and optically filtered to yield the $N_a - N_b$ or U field.

The technique of Scheme II will be reviewed below in connection with a specific example.

EXPERIMENTAL INVESTIGATION

Specimen and Specimen Grating

An isotropic disk in diametral compression was chosen as a test specimen. The disk was 50.8 mm (2 in.) in diameter and was machined from 9.5 mm (.375 in.) thick polymethylmethacrylate (PMMA) sheet stock. A phase grating with an aluminized-reflective coating was formed on the specimen surface. This was a cross-line grating of f = 600 lines/mm (15,240 lines/in.). The grating replication procedure used to form the grid on the specimen surface is described in detail in Part III of this dissertation.

Procedure

The specimen was placed in a loading fixture designed to apply compressive loading while minimizing rigid-body motions of the specimen. The loading frame, complete with specimen, was placed in the moiré interferometry system illustrated in Fig. 2.3. Angle α was adjusted to produce a virtual reference grating of 1200 ℓ/mm (30,480 ℓ/in.). A rotational mismatch between the specimen grating and virtual reference grating was introduced and orientation of the auxiliary mirror was adjusted, resulting in the three beams being converged on the aperture plate as shown in Fig. 2.5(a). Angular deviations between the three beams provided $C_x \approx C_{y_1} \approx C_{y_2} \approx 20$ lines/mm (510 lines/in.). All three beams were allowed to enter the camera and a no-load exposure was made on Film 1. A load was applied to the specimen and a second exposure was made on a second film, Film 2. All the raw data was acquired in this simple procedure.

After developing, Film 1 was placed in the optical filtering system where two exposures were made. The first consisted of combining beams a and b, as illustrated in Fig. 2.7, to obtain a fringe pattern of $N = N_a - N_b + C_1$, and was designated Film 3. The second exposure, on Film 4, was made of the interference pattern between beams a and -b, yielding $N' = N_a + N_b + C_2$. The load negative from the moiré interferometry system was then optically filtered in the same manner, resulting in two additional patterns of Films 5 and 6, respectively.

Films 3 and 5, with the no-load and load fringe patterns of the subtractive parameter, were superimposed and optically filtered to remove the carrier pattern, C_1, and enhance fringe contrast. The resulting moiré pattern of $N = N_a - N_b$, photographed as Film 7, represents contours of change of displace-

ment between the no-load and load exposures. In addition, since imperfections in gratings affect the load and no-load patterns equally, their influence is cancelled in this optical filtering operation. Finally, the optical filtering procedure was repeated using the superposition of Films 4 and 6, thereby obtaining Film 8, the moiré pattern of $N' = N_a + N_b$.

RESULTS AND DISCUSSION

The moiré fringe patterns resulting from the above procedure are shown as Figs. 2.8(a) and 2.8(b). Figure 2.8(a) is the easily recognized x-displacement field, the result of the subtractive moiré. Here, each fringe represents an in-plane displacement of 1/1200 mm or 0.833 μm (32.8 μin.). The out-of-plane displacement field resulting from the additive moiré is shown in Fig. 2.8(b). For the experiment conducted here, the green line of an Argon laser was used (λ = 514.5 nm), and $\alpha \approx 18$ deg. Substituting these values into Eq. 2.3 reveals that sensitivity to out-of-plane displacement was extremely high, approximately 0.132 μm per fringe (5.2 μin. per fringe). It should be noted that this is almost twice the sensitivity of normal-incidence holographic interferometry.

While the raw data is collected in a very easy and straightforward procedure, numerous optical filtering operations are required for data reduction. It would be attractive to find ways to eliminate the need for Films 3 through 6, but no direct method seems possible. These intermediate steps extract the sum and difference of wavefront warpages from the raw data before the final step of cancelling contributions of the no-load pattern. Optical filtering is seen as a very powerful data manipulation process, and considering its ability to perform the manipulations simultaneously throughout the full field of view, it is an efficient process.

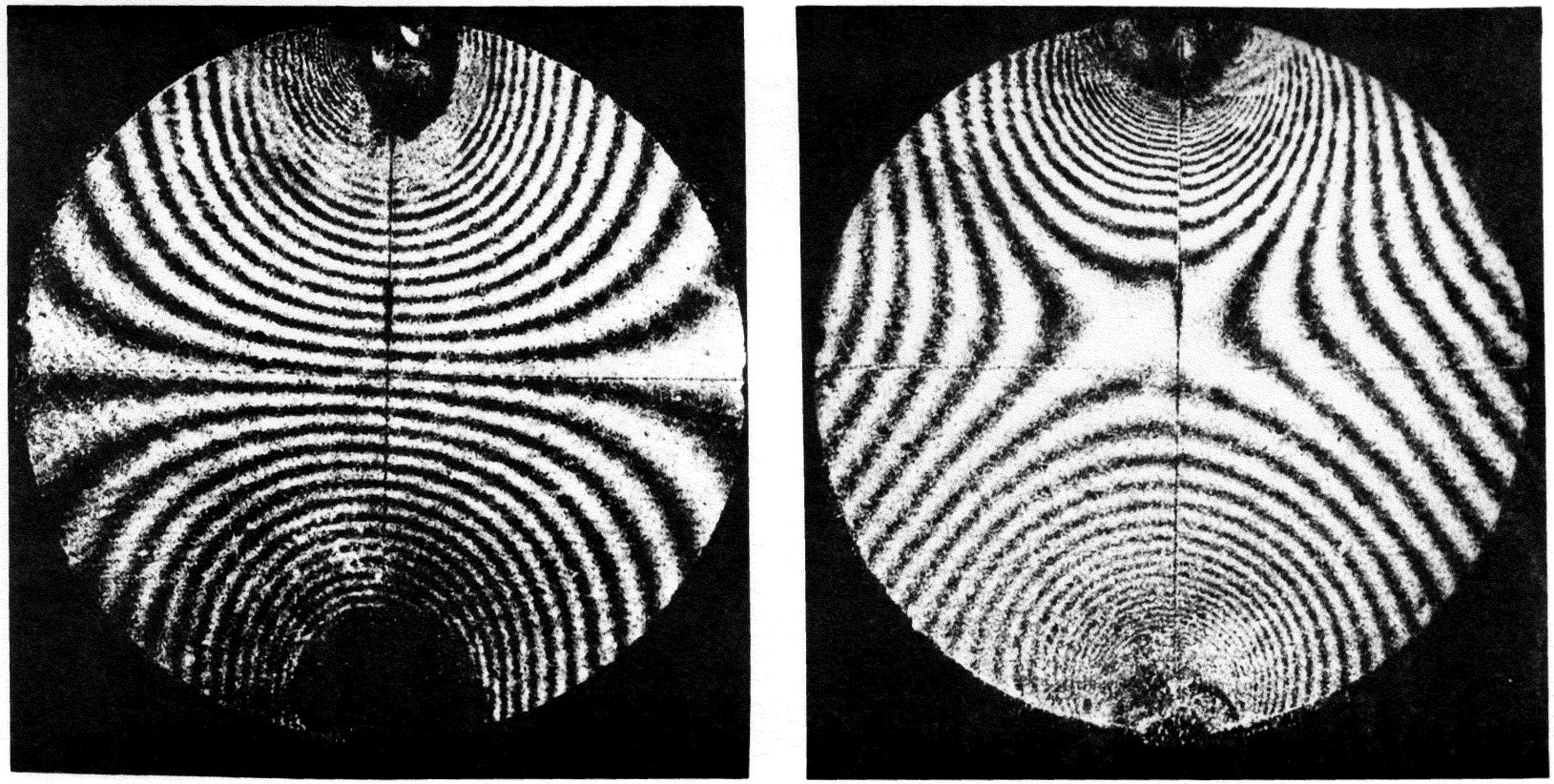

(a) (b)

FIGURE 2.8. THE RESULTS: PATTERNS OF (a) IN-PLANE AND (b) OUT-OF-PLANE DISPLACEMENTS FOR A DISK IN COMPRESSION. SLIGHT OUT-OF-PLANE RIGID-BODY ROTATION ACCOMPANIES THE DEFORMATION OF THE DISK

Although the experimental investigation performed for this work consisted of a static test, the simplicity of the technique lends itself to dynamic analyses. One must merely make an exposure containing the no-load information, followed by another exposure (or series of exposures) after the initiation of the dynamic event. These exposures can then be processed by optical filtering to determine the change of displacements at the instant of the dynamic exposure.

CONCLUSIONS

Effective means have been developed to reveal contour maps of the sum and the difference of wavefront warpages of beams emerging from a specimen grating. These depict out-of-plane and in-plane displacement fields, respectively, with very high sensitivities. With Scheme II, only a single photographic record is required for the load and another for the no-load condition. Data acquisition is experimentally simple and the method is amenable to dynamic as well as static analyses.

PART III

HIGH-FREQUENCY, HIGH-REFLECTANCE TRANSFERABLE MOIRÉ GRATINGS

SYNOPSIS--A technique has been developed whereby high-frequency moiré gratings with highly reflective surfaces can be transferred to work-pieces made from most engineering materials. Specimen gratings with frequencies as high as 2000 lines/mm (50,800 lines/in.) and exhibiting 10 percent diffraction efficiency in the first diffraction order have been applied to numerous specimens using simple laboratory techniques.

INTRODUCTION

The moiré method has been an attractive means of determining displacement fields for many years. It has wide application since it is a full-field technique that can be applied to the analysis of almost any engineering material for either static or dynamic investigations.

Of critical importance to the technique is the active or specimen grating. In earlier applications of the moiré method, practical considerations limited these gratings to 40 lines/mm (1000 lines/in.) or less. As a direct result, the sensitivity of measurements was severely limited. This drawback was circumvented by Post's method of moiré fringe multiplication, where coarse specimen gratings were used in conjunction with finer reference gratings to increase the sensitivity and accuracy of measurements by factors up to 60.[10,11] However, the light intensities of the higher diffraction orders used to obtain such patterns are tiny fractions of the incident light. It appears that fringe multiplication by a factor of 2 is optimal, but this requires specimen gratings of much higher frequencies, on the order of 500-2000 lines/mm (12,700-50,800 lines/in.).

Recently, methods have emerged to replicate such gratings unto specimens using a simple procedure.[1,12] Phase-type gratings are cast onto the workpiece using silicone rubber and a furrowed mold. Silicone rubber specimen gratings with a frequency of 600 lines/mm (15,240 lines/in.) have been used successfully in a number of investigations.[1,5,7,13] However, a foible of these gratings is the low reflectance of the surface, resulting in either long photographic exposure times or the use of a high-power laser. In addition, the transparency of the grating is sometimes troublesome, with reflections from specimen surface details generating noise in the moiré pattern. Greater reflection at the grating surface would suppress this unwanted signal and allow the use of relatively small, inexpensive lasers with output power of 1 mW or less.

Utilizing the technique for producing silicone rubber gratings as a foundation, the author has devised a procedure capable of transferring high-frequency gratings with highly-reflective surfaces to most engineering materials. It should be reiterated that the specimen gratings produced by this method are phase gratings, possessing a symmetrical corrugated surface which alters the phase of the incident light in a regular repetitive way. This is opposed to amplitude gratings, consisting of reflective bars and nonreflective spaces. The technique is described below.

GENERAL PROCEDURE

Before describing the exact details of the procedure, a more general overview is in order. A mold having a symmetrical furrow profile [Fig. 3.1(a)] of the desired frequency is fabricated. This mold is then placed in a vapor deposition unit where it is overcoated with a very thin layer of a metallic material which

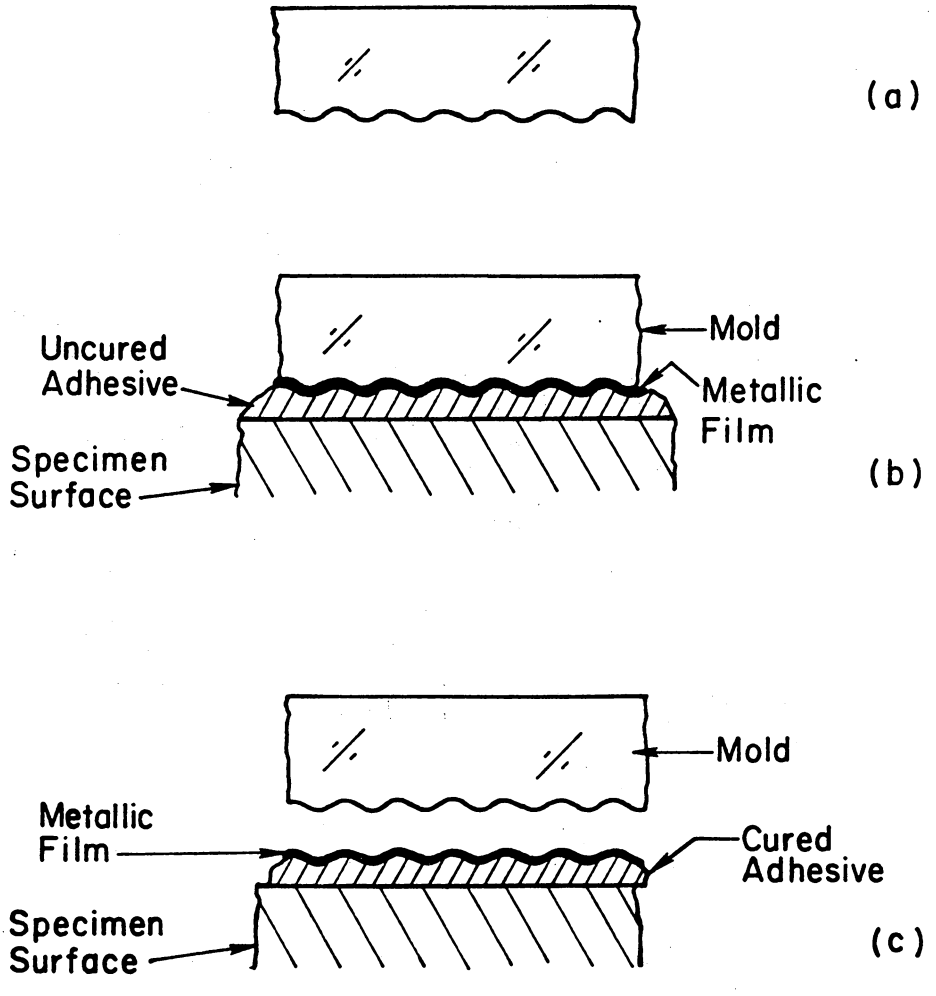

FIGURE 3.1. STEPS IN FORMING THE SPECIMEN GRATING

possesses a high degree of reflectivity. The coated mold is used to produce a specimen grating in an adhesive material by squeezing out a film of the adhesive between the mold and the specimen. This is illustrated in Fig. 3.1(b). The adhesive film is cured.

If an attempt is made to remove the mold, separation can occur at three interfaces; (1) between the specimen and the adhesive, (2) between the adhesive and the metal film, and (3) between the metal film and the mold. Tests conducted during the current investigation indicate that the use of certain adhesives can insure separation at the third interface, between the metal film and the mold. This is the desired result, yielding a phase-type specimen grating with a high-reflectance coating [Fig. 3.1(c)].

DETAILED PROCEDURE

Step 1 - Mold Fabrication

The mold must contain a symmetrical corrugated surface as illustrated in Fig. 3.1(a). Using simple laboratory and darkroom techniques, high-resolution photographic plates can be processed to exhibit the desired profile.

If two collimated beams of light are caused to interfere as illustrated in Fig. 3.2, a three-dimensional pattern of constructive and destructive interference is formed in space in the hatched zone where the beams cross at angle 2α. This is a steady-state phenomenon, consisting of closely spaced horizontal walls of destructive interference, each separated by a distance, g, known as the pitch. The frequency f (where $f = 1/g$) of this "virtual" grating depends upon the angle α according to the relationship,

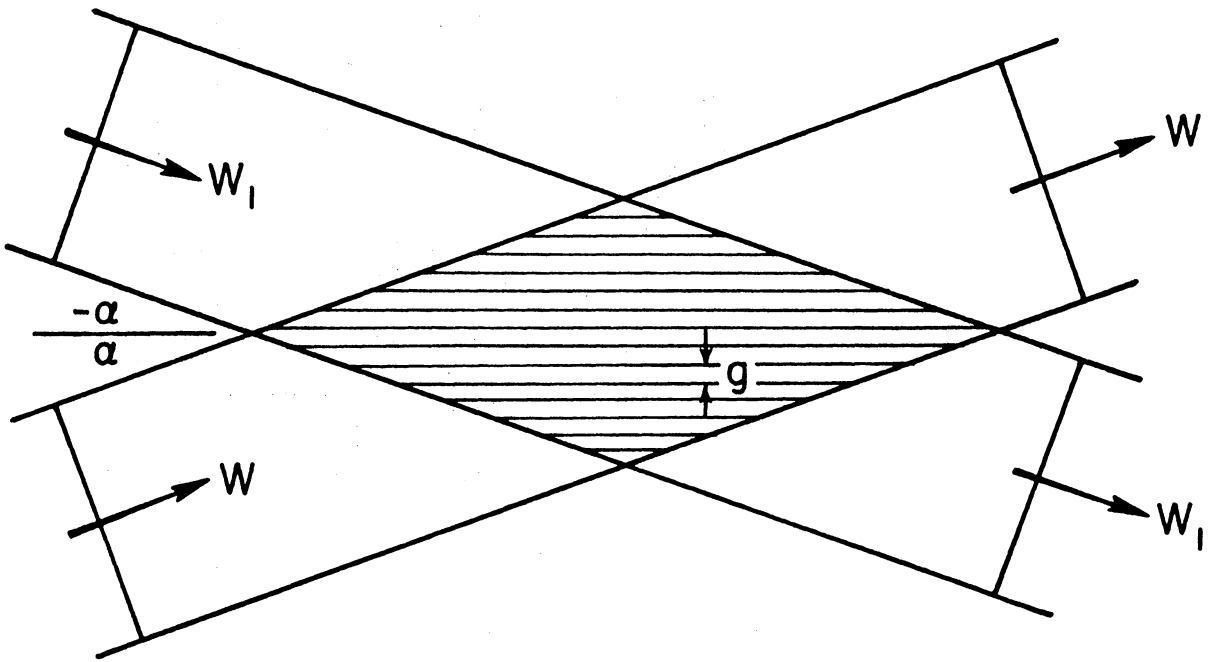

FIGURE 3.2. INTERFERENCE OF TWO COHERENT BEAMS FORMS A VIRTUAL GRATING OF FREQUENCY f

$$\sin \alpha = \frac{f}{2}\lambda \qquad (3.1)$$

where λ is the frequency of the light used.

An apparatus shown schematically in Fig. 3.3 is used to generate the interference pattern described above. Angle α is adjusted to form a virtual grating of the desired frequency, the frequency being related to angle α as given in Eq. 3.1. (The adjustment procedure is included as Appendix A.)

A photographic plate is installed in the plate holder and an exposure is made. When the plate is developed (see Appendix B for development steps), silver grains remain in the zones exposed to constructive interference, while the silver is leached out of the gelatin in the zones of destructive interference. This is illustrated in Fig. 3.4(a). The gelatin matrix shrinks upon drying, but it is partially restrained by the silver, resulting in the corrugated surface of Fig. 3.4(b). This surface serves as the mold for the phase grating.

The depth of the furrows, and therefore the diffraction efficiency of the grating, can be controlled by the exposure time. For the reflective moiré technique, light from the +1 and -1 diffraction orders of the specimen grating is used. For this reason, an exposure time is desired which will result in the grating having the greatest efficiency in the first order. During the current investigation, numerous plates with different exposure times were processed as per Appendix B. The plates were then coated with a thin aluminum film in a vapor deposition unit and the first order diffraction efficiencies were measured and compared. The exposure time corresponding to the greatest diffraction efficiency was used.

The corrugation effect can be further enhanced by bleaching the plates during processing. As shown in Appendix B, the bleaching step follows develop-

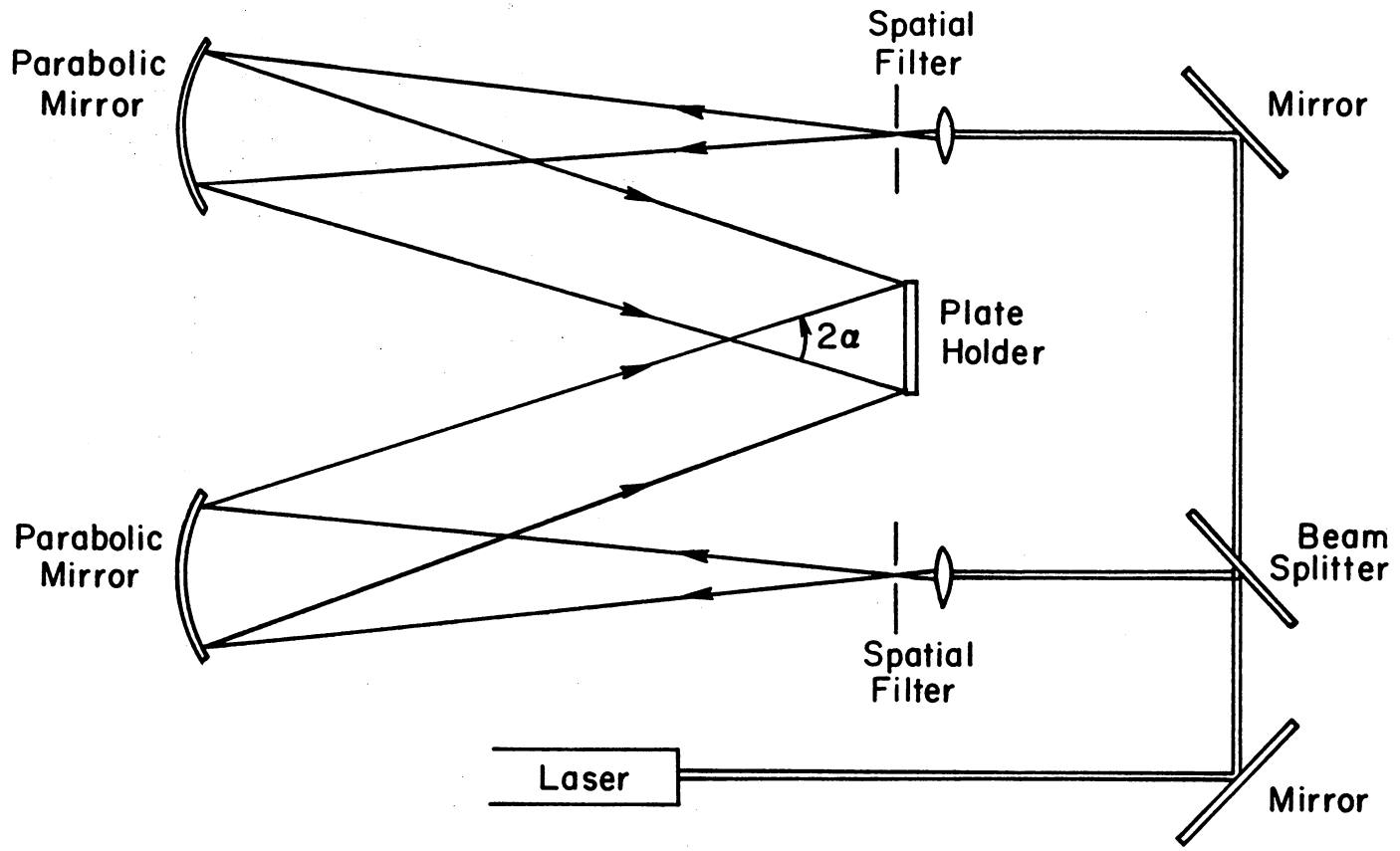

FIGURE 3.3. APPARATUS USED TO GENERATE THE VIRTUAL GRATING. A PHOTOGRAPHIC PLATE IS PLACED IN THE HOLDER AND EXPOSED TO OBTAIN A GRATING OF FREQUENCY f, WHERE $f = (2 \sin \alpha)/\lambda$

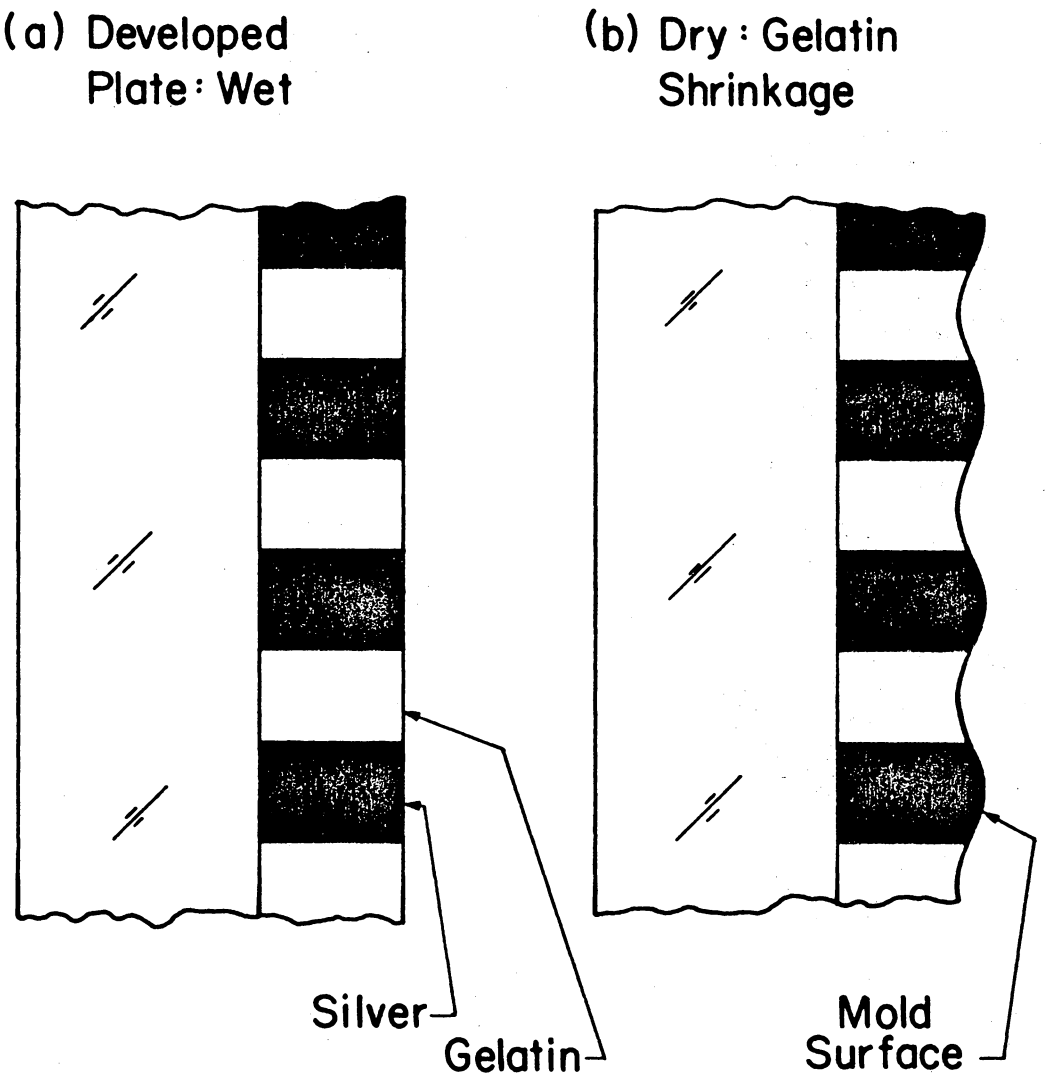

FIGURE 3.4. FORMATION OF CORRUGATED SURFACE IN PHOTOGRAPHIC PLATE BY SHRINKAGE OF GELATION

ment and fixing of the plate, where it converts the developed metallic silver grains into transparent dielectric deposits. According to Benton,[14] cross-linking effects between the gelatin and the bleach byproducts cause the gelatin to "heave", thereby increasing the depth of the zones which originally contained the silver grains.

The green-line of an Argon laser was used in the set-up of Fig. 3.3, prompting the use of Kodak HRP-TE photographic plates which are green-sensitive. The 102 mm x 102 mm (4 in. x 4 in.) plates were obtained from IMTEC Products, Inc. of Sunnyvale, California. Previous efforts using a He-Ne laser and Kodak Holographic Plate, Type 120-02 also achieved good results,[1] although diffraction efficiencies were lower. For the particular set-up illustrated in Fig. 3.3, with 152 mm (6 in.) diameter, 1.22 m (48 in.) focal length parabolic mirrors, spatial filters containing 40X microscope objectives and 5 micron pinholes, and a laser power of 100 mW; the optimal exposure time for Kodak HRP-TE plates was 2.5 seconds for a linear grating. Of course, if a cross-line grating is desired, the plate can be rotated 90 degrees, followed by a second exposure. In this case, an exposure time of 2 seconds for each exposure appears optimal.

Step 2 - Overcoating the Mold

Aluminum was chosen as the reflective overcoat because of its high reflectivity in thin films, low adhesion to the developed photographic plate, and its ability to resist tarnishing. Test results show gold to be an excellent substitute but the accessibility and lower cost of aluminum made it more attractive for the numerous tests conducted during this investigation.

An additional requirement of the metallic film is that it must not contribute a significant reinforcing effect to the specimen. This requirement, and the use of some ultraviolet curing adhesives in the final step of the replication process (where the ultraviolet rays must pass through the film to cure the adhesive), led to the choice of a film thickness yielding 50% reflectance of light. The thickness of an aluminum film with this characteristic is approximately 100 nm. However, this is by no means an exacting quantity and efforts to achieve a film of a specific thickness are not required. Instead, the simple technique illustrated in Figure 3.5 can be used to monitor the reflectance of the coating during the evaporation procedure.

A processed photographic plate is cut to the desired dimensions and attached to a holding plate. This plate is suspended in a vapor deposition unit approximately 25 cm (10 in.) above a tungsten coil containing a small piece of aluminum wire. The holding plate contains an aperture and a mirror system such that the tungsten coil can be viewed simultaneously through the aperture and through the mold. A mold containing a coating that is known to exhibit 50% reflection is placed in the viewing path at point A in Fig. 3.5. A shield at B prevents the deposition of aluminum on the bell jar in the viewing path of the operator.

The chamber is evacuated to less than 10^{-5} torr, and current is passed through the tungsten filament. The glowing filament is viewed simultaneously through the mold with the known coating and the photographic plate being coated. As the aluminum evaporates, the intensity of the light from the filament is visually monitored until the densities of the two coatings appear nearly equal. At this point, the current to the tungsten filament is shut off. The reflectance of

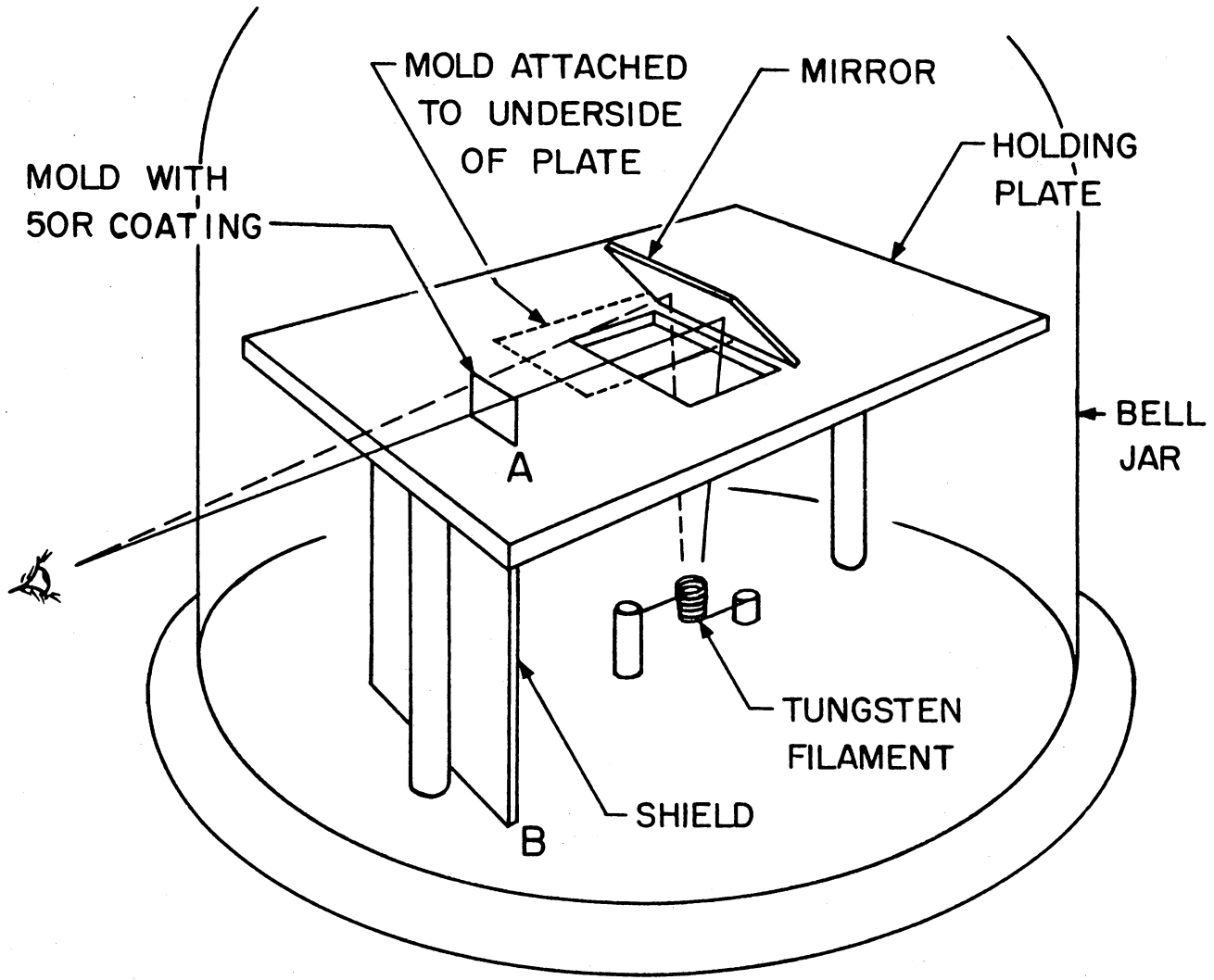

FIGURE 3.5. SCHEMATIC OF VAPOR DEPOSITION UNIT AND APPARATUS USED TO OBTAIN 50% REFLECTIVE COATINGS ON THE MOLD

several plates coated in this manner has been measured, and suitable results were obtained. It should be noted that the mirror positioned above the aperture is also coated during the evaporation process. However, this does not affect its reflective properties.

The overcoated mold should be handled carefully and stored in a dust free environment to insure that the metallic surface is not contaminated prior to the bonding operation.

Step 3 - Specimen Grating Fabrication

In this step, the corrugated surface of the mold is replicated on the specimen, as illustrated in Fig. 3.1. Although initial preparation of various adhesives may vary, the bonding operation remains basically the same. The surface of the specimen is prepared by initial roughing with 600 grit sandpaper, solvent cleaning, and one final pass with new 600 grit sandpaper to remove all traces of solvent residue and insure a clean surface. The uncured adhesive is poured as a puddle on the specimen and the overcoated mold is placed over the specimen and weighted to squeeze out excess liquid. The pressure required is dependent upon the viscosity of the particular adhesive being used, but should be sufficient to yield a final grating thickness of approximately .025 mm (.001 in.). When the adhesive has cured to the consistency of hard rubber, excess adhesive can be cleaned from the specimen mechanically and with the use of recommended solvents. After complete curing of the adhesive, the mold is lifted off.

During the course of this investigation, several epoxies and adhesives were evaluated. Of all the epoxies tested, PC-10C and PC-6C, manufactured by

Measurements Group, Raleigh, NC, appear to achieve the best results. It is probable that other epoxies on the market would yield similar results. Two ultraviolet curing acrylic adhesives, NOA 61 and NOA 65, manufactured by Norland Products, Inc. of New Brunswick, NJ were also found to give good results. Properties of these four adhesive systems which may be pertinent for various applications are listed in Table 3.1. Specific handling and curing procedures required for the epoxies and optical adhesives are described below.

Epoxies: Two major concerns exist with the use of epoxies as the grating material: (1) removal of all air bubbles introduced during mixing, and (2) prevention of moisture absorption during the mixing and application steps. Both the introduction of air bubbles and moisture absorption result in local defects or voids in the finished grating. These two problems can be avoided by keeping the individual components and the final mixture at an elevated temperature of approximately 130-140°F until it is poured on the specimen. This increased temperature decreases the viscosity of the constituents and the final mixture and allows easier removal of air bubbles. In addition, the elevated temperature drives off any moisture present and prevents further condensation.

The resin and hardener are heated separately. The appropriate proportions are weighed out, followed by thorough mixing. The epoxy is poured into a warm test tube and centrifuged at 3500 rpm for 2-3 minutes to remove air bubbles. The epoxy is reheated to remove any remaining moisture before pouring it on the specimen. To achieve a grating thickness of .025 mm (.001 in.), the mold must be weighted with approximately 9-12 kPa (1 1/2 - 2 lb/in^2).

TABLE 3.1. PROPERTIES AND CURE TIMES OF EPOXIES AND ACRYLICS

Epoxy or Acrylic	E, kPa (ksi)	Elongation %	Maximum Temp., °C (°F)	Cure Time at Room Temp.*
PC-10C	3100(450)	3-5	80(180)	3-4 hrs
PC- 6C	210(30)	50	205(400)	24 hrs
NOA-61	1030(150)	38	175(350)	20 min
NOA-65	140(20)	80	175(350)	20 min

* Time of cure for the optical adhesives is dependent on the intensity of U.V. light, the thickness of the adhesive layer, and the U.V. transmission of the mold. The cure times stated above are for a .025 mm (.001 in.) or less adhesive layer placed 25 cm (10 in.) from a 250 watt high-intensity mercury vapor lamp using molds fabricated as per the previous section.

Optical Adhesives: The optical adhesives used here offer the advantages of shorter curing times and less complicated handling procedures. Both NOA 61 and NOA 65 are one part systems, thus no mixing is required and no air bubbles are introduced. The viscosity of these adhesives is an order of magnitude less than the epoxies, resulting in less weight being required to achieve the desired grating thickness.

After the adhesive is poured on the specimen, the mold is placed over it and weighted with approximately 3 kPa (1/2 lb/in^2). The weight is removed and the adhesive is cured in a setup such as illustrated in Fig. 3.6, where a 250 watt high-intensity mercury vapor lamp is used as a source of ultraviolet radiation to cure the adhesive. The total distance from the lamp to the specimen is 25 cm (10 in.) resulting in a complete cure time of about 20-25 minutes.

RESULTS AND DISCUSSION

Using the techniques described above, reflective specimen gratings of excellent quality were obtained. Both linear and cross-line gratings with frequencies varying from f = 600 lines/mm to f = 2000 lines/mm (15,240 lines/in and 50,800 lines/in, respectively) were produced using the four adhesive systems chosen. Tests were completed on specimens made from 7075 aluminum, cold-rolled steel, polymethylmethacrylate (PMMA) and T300/934 graphite/epoxy, each displaying excellent results for all four of the adhesive systems. In addition, gratings fabricated using NOA 61 have been utilized for the investigation reported in Part II of this dissertation, and for work being conducted by Weissman and Post,[15] where sensitivities to displacement as high as 1/4000 mm per fringe (1/101,600 in. per fringe) have been recorded.

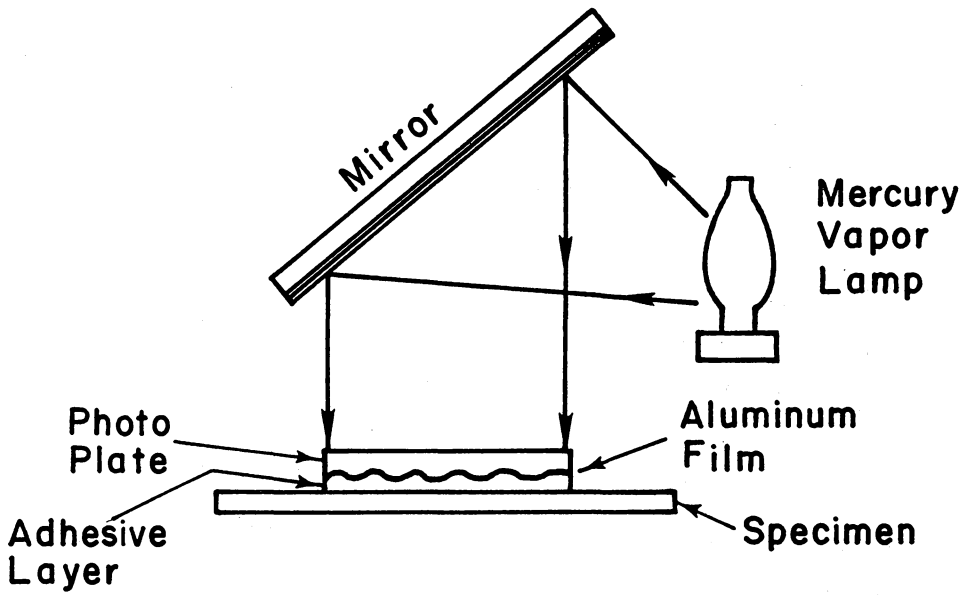

FIGURE 3.6. APPARATUS USED TO CURE THE OPTICAL ADHESIVE AND FORM THE SPECIMEN GRATING

In an effort to compare the gratings obtained using this technique with the silicone rubber gratings used previously, first order diffraction efficiencies were measured for both types of linear gratings. All gratings were made from photographic plates processed according to Appendix B. Defining diffraction efficiency as the ratio of the light intensity emerging in the +1 or -1 diffraction order and the intensity of the incident light, the average values obtained were 0.25% for silicone rubber gratings and 10.0% for the aluminized gratings. This significant increase was observed for gratings made with each of the four adhesive systems tested, with no one adhesive exhibiting superior results over the others.

Although the use of these four adhesives did insure separation at the interface between the aluminum film and the mold, several attempts were made to further reduce the adhesion at this interface. A rather simple procedure that achieves this result involves the use of Kodak Photo-Flo as the last step in the plate processing procedure (see Appendix B). This apparently leaves a very thin, uniform film of contaminant on the dry surface which interferes with strong adhesion of the aluminum layer. Test results indicated that plates processed in Photo-Flo could be separated from the grating with less force than was required when no Photo-Flo was used. It is therefore recommended that this step be included in the processing procedure.

SUMMARY AND CONCLUSIONS

Moiré interferometry has evolved into a technique capable of determining in-plane and out-of-plane displacements with a high degree of sensitivity. Use of

this method has created a need for improved high-frequency specimen gratings exhibiting highly reflective surfaces.

A technique has been developed whereby specimen gratings with reflective coatings and frequencies up to 2000 lines/mm (50,800 lines/in.) can be transferred to the surface of specimens made from most engineering materials. This method is quite simple and general and should prove useful in many applications of moiré interferometry.

SUMMATION AND RECOMMENDATIONS

It has been shown that wavefront warpage induced by specimen deformation provides sufficient information to determine both in-plane and out-of-plane displacement fields. In addition, an experimental technique has been developed which allows simultaneous determination of both of these fields. The method requires only one photographic exposure of the deformed specimen, with displacement information being extracted through the use of optical filtering. Finally, a procedure has been developed for producing high-frequency specimen gratings with highly reflective surfaces.

The major objective of this work has been to develop an experimental technique capable of simultaneously determining in-plane and out-of-plane displacements. To date, the resulting technique has not been utilized in a problem solving situation. Therefore, it is suggested that the actual merits of the method can only be appreciated after it has been used in this capacity.

REFERENCES

1. Post, D. and Baracat, W. A., "High-Sensitivity Moiré Interferometry--A Simplified Approach", Experimental Mechanics, 21(3), pp 100-104 (March 1981).

2. Hung, Y. Y., "Displacement and Strain Measurement", Speckle Metrology, R. K. Erf, Editor, Academic Press (1978).

3. Parks, V. J., "The Range of Speckle Metrology", Experimental Mechanics, 20(6), pp 181-191 (June 1980).

4. Beranek, W. J. and Bruinsma, A. J. A., "A Geometrical Approach to Holographic Interferometry", Experimental Mechanics, 20(9), pp 289-300 (Sept. 1980).

5. Weissman, E. M. and Post, D., "Full Field Displacement and Strain Rosettes by Moiré Interferometry", Proceedings of the 1981 Spring SESA Meeting, May 31-June 4, Dearborn, MI.

6. Sciammarella, C. A., Di Chirico, G., and Chang, T. Y., "Moiré Holographic Technique for Three-Dimensional Stress Analysis", Journal of Applied Mechanics, pp 180-185 (March 1970).

7. Basehore, M. L. and Post, D., "Moiré Method for In-Plane and Out-of-Plane Displacement Measurements", Experimental Mechanics, 21(9), pp 321-328 (Sept. 1981).

8. Durelli, A. J., and Parks, V. J., "Moiré Fringes as Parametric Curves", Experimental Mechanics, 7(3), pp 97-104 (March 1967).

9. Ostrovsky, U. I., Butusov, M. M., and Ostrovskaya, G. V., Interferometry by Holography, Springer-Verlag, Berlin, 1980, pp 186-192.

10. Post, D., "Analysis of Moiré Fringe Multiplication Phenomena", Applied Optics, 6(11), pp 1938-1942 (Nov. 1967).

11. Post, D., "Moiré Fringe Multiplication With a Nonsymmetrical Doubly Blazed Reference Grating", Applied Optics, 10(4), pp 901-907 (April 1971).

12. Post, D., "Optical Interference for Deformation Measurements--Classical, Holographic and Moiré Interferometry", Mechanics of Nondestructive Testing, W. W. Stinchcomb, Editor, Plenum Publishing Corp., New York (1980).

13. Watson, R. B. and Post D., "Precision Strain Standard by Moiré Interferometry for Strain Gage Calibration", Proceedings of the 1981 SESA Spring Meeting, May 31-June 4, Dearborn, MI.

14. Benton, S. A., "Photographic Materials and Their Handling", Handbook of Optical Holography, H. J. Caulfield, Editor, Academic Press, New York (1979).

15. Weissman, E. M. and Post, D., Personal Communication (Aug. 1981).

APPENDIX A

The following procedure is used to align the optical system of Fig. 3.3 (reproduced here as Fig. A.1) to obtain an interference pattern of the desired frequency.

I.) Roughly align the optics for the desired frequency according to the relationship,

$$\sin \alpha = \lambda \frac{f}{2} \tag{A.1}$$

where angle α is illustrated in Fig. A.1. (In effect, the sum of these angles will be adjusted to 2α.)

II.) Insert a real diffraction grating (transmission grating) in the plate holder illustrated in Fig. A.1, orienting the grating lines as closely as possible to vertical. If the frequency of the real grating is denoted by f', then f' must be related to the desired frequency, f, by;

$$f' = \frac{1}{n} f \tag{A.2}$$

where n is an integral number. For practical purposes, n should have a value of 5 or less.

The effect of the real grating is illustrated in Fig. A.2 for the case of n = 4. If the diffraction orders from plane wavefronts WF_1, and WF_2 are denoted by r and s, respectively, wavefronts emerging in the diffraction orders which satisfy the equation

$$n = s - r \tag{A.3}$$

will be coplanar if the system is precisely aligned. Two factors that can contribute to the misalignment are

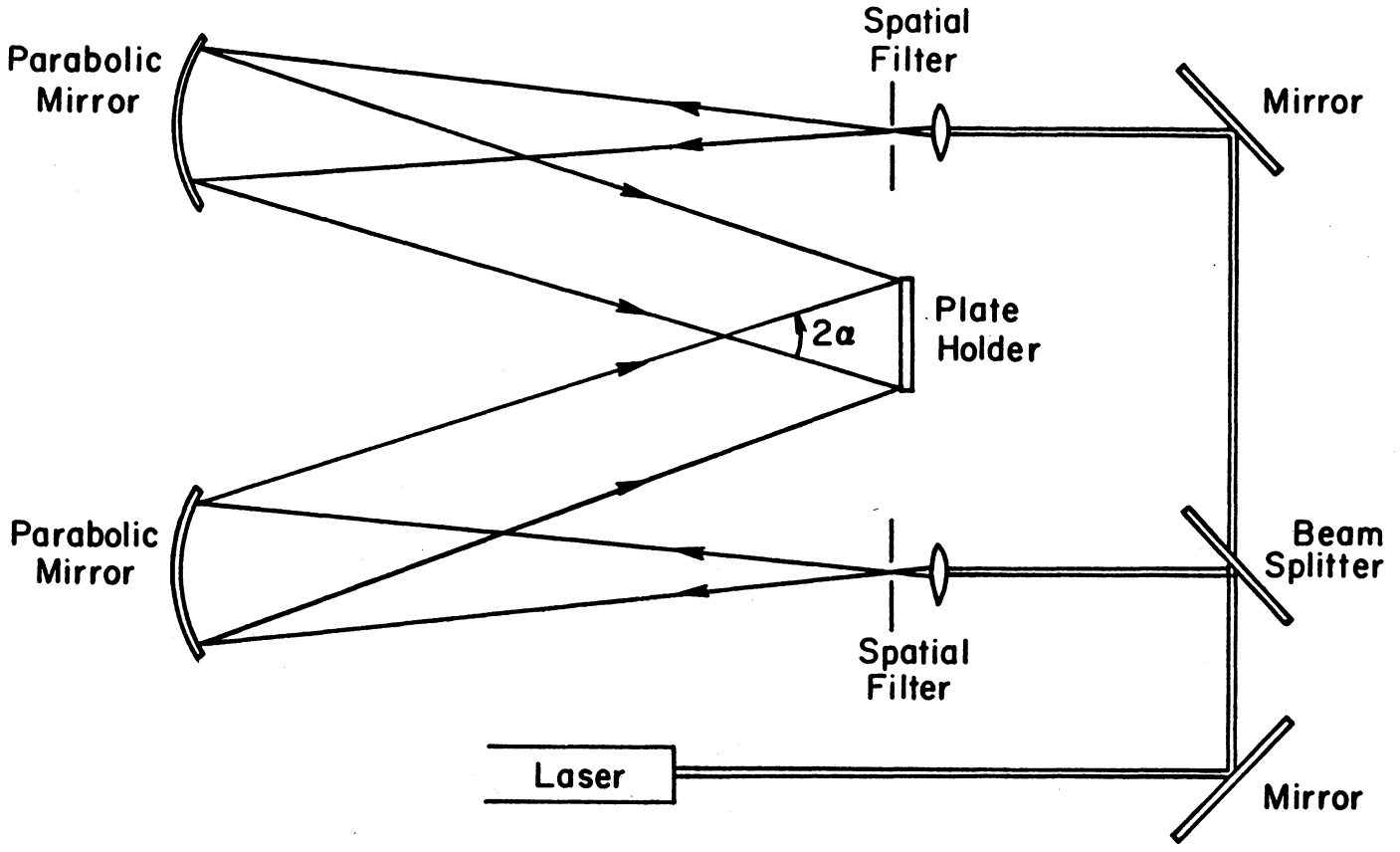

FIGURE A.1. APPARATUS USED TO GENERATE THE VIRTUAL GRATING. A PHOTOGRAPHIC PLATE IS PLACED IN THE HOLDER AND EXPOSED TO OBTAIN A GRATING OF FREQUENCY f, WHERE $f = (2 \sin \alpha)/\lambda$

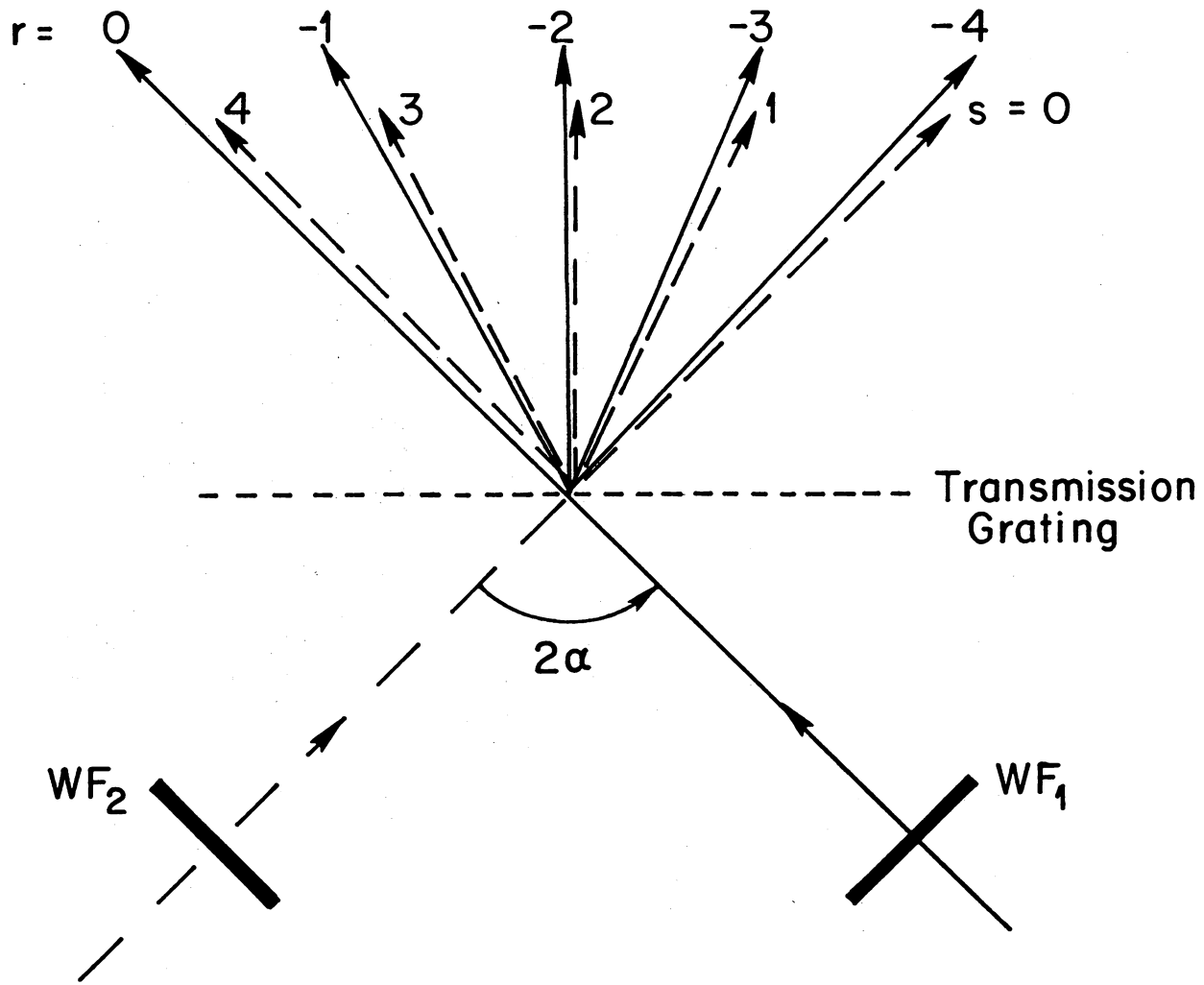

FIGURE A.2. RAY DIAGRAM ILLUSTRATING THE DIFFRACTION ORDERS GENERATED BY A REAL GRATING PLACED IN THE PLATE HOLDER OF FIG. A.1, FOR n = 4

1.) angle α may not satisfy Eq. A.1 and

2.) lines on the real and virtual gratings may not be parallel.

It is merely a matter of correcting these two factors to achieve exact alignment of the system.

III.) To do this, place a convex lens behind the real grating so as to observe any two diffraction orders which satisfy Eq. A.3. Two points of light should be visible in the focal plane of the lens, their separation being a function of the degree of misalignment.

IV.) Rotate the real grating about an axis normal to its surface until the two points of light are on the same horizontal line. The lines of the real grating and the virtual grating are now roughly parallel.

V.) Adjust angle α (or 2α) until the two points of light appear to be in total registration.

VI.) "Fine tuning" of the angle adjustment is accomplished as follows. View the coincident diffraction orders in any plane other than the focal plane of the convex lens. Unless the wavefronts of the diffracted beams are in perfect registration, a fringe pattern will be observed. Once again, rotate the real grating, this time until the fringes in the pattern are vertical. This step eliminates rotational mismatch between the real and virtual gratings. The remaining fringe pattern is the result of a frequency mismatch between the real and virtual grating (i.e., the frequency of the desired virtual grating is not a precise integral multiple of the real grating). Adjust angle α until the closest approach to a null field is observed. The optical system is then aligned.

APPENDIX B

The following procedure is used for processing Kodak HRP-TE plates.

1.) Develop for 4 min. in HRP developer (1:4).

2.) Wash in running water for 15-30 secs.

3.) Fix, using Kodak Fixing Bath F-24, for double the visible clearing time.

4.) Wash in running water for 15-30 secs.

5.) Hypo Clearing Agent for 1 min.

6.) Wash in running water for 30 secs.

7.) Bleach, using Kodak Bleach R-10, for double the visible clearing time.

8.) Wash in running water for 3 min.

9.) Kodak Photo-Flo for 30 secs.

10.) Dry vertically in still, room temperature air.

All handling of plates after the completion of Step 8 should be done with plastic gloves to avoid contamination by finger oils. Directions for preparing the fixer and bleach used in the above processing are given in Appendix C.

APPENDIX C

The following steps should be used for the preparation of Kodak Fixing Bath F-24 and Kodak Bleach R-10.

Fixer F-24

Water about 125° F (50° C)	1900 cc
Sodium thiosulfate	912 g
Sodium sulfite, dessicated	38 g
Sodium bisulfite	95 g
Cold water to make	3.8 ℓ (1 gallon)

Dissolve chemicals in the order given.

Bleach R-10

Solution A		Solution B	
Ammonium dichromate	20 g	Potassium bromide	92 g
Sulfuric acid	14 mℓ	Water	1 ℓ
Water	1 ℓ		

Prepare stock solutions A and B for storage. When ready for use, mix equal parts of solutions A and B with 10 parts water.

The vita has been removed from the scanned document

MOIRÉ INTERFEROMETRY FOR OUT-OF-PLANE DISPLACEMENT MEASUREMENTS

by

Michael L. Basehore

(ABSTRACT)

Moiré interferometry is a relatively new branch of photomechanics that utilizes a diffraction grating on the specimen to determine surface displacements. To date, it has been used primarily to determine in-plane displacements of the specimen surface. The objective of this work is to demonstrate that the technique is capable of determining out-of-plane displacements as well.

A high-frequency phase grating on a specimen surface is illuminated by oblique beams; two diffracted beams are recorded by holographic interferometry. If the wavefront warpages of the two diffracted beams are characterized by fringe orders, N_a and N_b, it is demonstrated that the in-plane displacements are proportional to $N_a - N_b$, while out-of-plane displacements are proportional to $N_a + N_b$. Initially, these subtractive and additive parameters are determined numerically, and the resulting displacements are compared to displacements measured by well-accepted prior experimental methods. Excellent agreement with these proven methods is shown.

Using this remarkably simple relationship between wavefront warpages, an experimental procedure is developed which is capable of simultaneously determining the in-plane and out-of-plane displacements of a specimen surface. The method requires only one photographic exposure of the deformed specimen, with

displacement information being extracted through the use of optical filtering. The fact that the information required to yield these patterns can be obtained from a single photographic recording not only makes this an experimentally simple technique to use, but provides the capability of analyzing dynamic events as well.

The sensitivity of measurements made by utilizing this technique are directly proportional to the frequency of the specimen grating. Therefore, it is desirable to obtain specimen gratings with frequencies on the order of 500-2000 lines/mm (12,700 - 50,800 lines/in.). A technique is developed whereby high-frequency moiré gratings with highly reflective surfaces can be transferred to workpieces made from most engineering materials. Specimen gratings with frequencies as high as 2000 lines/mm (50,800 lines/in.) and exhibiting 10 percent diffraction efficiency in the first diffraction order have been applied to numerous specimens using simple laboratory techniques.